Performance Analysis of Point-to-Multi-Point ($P2MP$) Hybrid FSO/RF Network

by

Alwa Mohamed Boharba
B.Sc., Al Zawia University, 2010

A Thesis Submitted in Partial Fulfillment of the
Requirements for the Degree of

MASTER OF APPLIED SCIENCE

in the Department of Electrical and Computer Engineering

Performance Analysis of Point-to-Multi-Point ($P2MP$) Hybrid FSO/RF Network

by

Alwa Mohamed Boharba
B.Sc., Al Zawia University, 2010

Supervisory Committee

Dr. Fayez Gebali, Supervisor
(Department of Electrical and Computer Engineering)

Dr. Kin Fun Li, Departmental Member
(Department of Electrical and Computer Engineering)

Supervisory Committee

Dr. Fayez Gebali, Supervisor
(Department of Electrical and Computer Engineering)

Dr. Kin Fun Li, Departmental Member
(Department of Electrical and Computer Engineering)

ABSTRACT

In this thesis, we present a detailed analysis of hybrid point-to-multipoint free space optical (FSO)/radio frequency (RF) wireless system. Hybrid FSO/RF systems have emerged as a promising solution for high data rate wireless transmission. FSO technology can be used effectively in multiuser scenarios to support Point-to-Multi-Point (P2MP) networks. In this P2MP network, FSO links are used for data transmission from a central location to multiple users. When more than one FSO link fail, the central node uses a common backup RF link to transmit a frame to a remote node using an equal priority protocol. An equal priority protocol means that the remote nodes have the same priorities in being assigned the RF link. We assume two traffic classes, a high-priority and low-priority classes. The base station reserves two transmit buffers of each user for the downlink transmission. Considering the downlink traffic from the base station to a tagged remote node, we study several performance metrics. We develop a cross-layer Markov chain model to study the throughput from central node to a remote node as well as the performance of the resulting system.

Contents

List of Figures

List of Acronyms

FSO	Free Space Optical
LOS	Line-of-Sight
LTE	Long-Term Evolution
MIMO	Multiple-input Multiple-output
MMW	Milli-Meter Wavelength
MRC	Maximal Ratio Combining
OSSK	optical space shift keying
OWC	Optical wireless communication
P2MP	Point-to-Multi-Point
P2P	Point-to-Point
QoS	Quality of Service
RF	Radio Frequency
SNR	Signal-to-Noise Ratio
SAN	Storage area network
UV	Ultra Violet
VLC	Visible Light Communication
WISP	Wireless Internet Service Provider
WiFi	Wireless Fidelity

ACKNOWLEDGEMENTS

In the name of Allah, the most Gracious, the most Merciful. All praise be to Allah the Almighty who has given me knowledge, patience, and perseverance to complete my Master's dissertation.

My sincere thanks to my parents; my father Mr. Mohamed Aboharba and my mother, Mrs. Zuhra Almaqtouf for their emotional support, encouragement, and prayers, continuous guidance, deepest love, assurance during my tough times, and blessings over all these years.

I would like to express my appreciation to my supervisor Dr. Fayez Gebali for his invaluable scholarly advice, inspiration, help, support and guidance that helped me through my Master's dissertation work. It is a pleasure to acknowledge his guidance and support. Thank you very much for being such a fantastic supervisor.

I am extremely grateful to my lovely husband Malek Elgadi for his support, help, efforts, continuous guidance, deepest love, and assurance during my tough times.

I am heartily thankful to Dr. Mohammed Shoukry for his support, help, encouragement, continuous guidance, and assurance during my tough times. I am really grateful to him and I cannot find the words to adequately describe what he has done for me. He never let me down at any moment. Instead, he convinced me that I can persist more to reach my goals no matter what obstacles lie in my way. I can only say thank you from the bottom of my heart and I know it is not enough at all.

I would like to acknowledge the advice and support from my supervisory committee's members: Dr. Kin Fun Li, Dr. Keivan Ahmadi, as well as the external examiner, Dr. Esam Abdel-Raheem: for making my dissertation complete and resourceful.

I am heartily thankful to my brother Khalid Aboharba for his support, help, efforts, motivation and assurance during my tough times. I am extremely grateful to my siblings, Taqwa Aboharba, Yosra Aboharba, Bushra Aboharba, Salem Aboharba, Oqba Aboharba, and Salah-eldeen Aboharba for their invaluable support and enlightening discussions. They have provided me with so much help, love, and valuable advice.

I feel a special gratitude to Sumaya Atewah for her invaluable support, continuing encouragement, and enlightening discussions.

I am extremely grateful to Amina Mohamed and Mentalla Abdelhamid for their help, guidance, and encouragement.

I would like to give special thanks to Najah Aldreak, Sundus Nasrat, Daida Mersal, Amal Gaber, and Samia Benhmeda for their guidance, support, and beneficial discussions.

I would like to give special thanks to Fatma Ahmeda, and Hana Alqadafi for their help, support and generous friendship, as well as Noman Lashari for his availability and enlightening discussions.

Alwa Mohamed Salem Aboharba, Victoria, BC, Canada

DEDICATION

To my parents; my father Mr. Mohammed Aboharba and my mother, Mrs. Zuhra Almaqtouf for their deepest love, continuous guidance, dedication, and prayers. To my lovely husband; Malek Elgadi, my sons: Abdulrhman and Mohammed, my sisters and my brothers for their encouragement, support, and deepest love.

Chapter 1

Introduction

1.1 Overview

Optical Wireless Communication (OWC) is a technology that requires the transmission of information-laden optical radiation over the free space channel.

Recently, the interest of the optical wireless communication (OWC) as a promising technology in short-range communications has grown mainly because of the need for higher data rates in support of communication applications [5]. It offers flexible networking solutions that give high-speed broadband connectivity, also cost-effective for indoor and outdoor applications [6].

OWC is classified into three main types, which are Free-Space Optical (FSO) communications, Visible Light Communications (VLC), and Ultra-Violet (UV) Communications [7]. Free space optical (FSO) communication has attracted significant attention due to its advantages, such as large usable and unlicensed bandwidth, long operational range, spatial re-usability, security, and immunity to electromagnetic interference [5].

Despite of the great potential of the FSO link, FSO links face fading problems because of atmospheric turbulence [8]. It also suffers from multiple impairments, such as severe path-loss effect, pointing error degradation, and line-of-sight (LOS) needs. Also atmospheric weakness such as an atmospherics turbulence and visibility-limiting conditions (snow, fog, and dust), which undermines the reliability of FSO links, and may lead to deterioration in performance (outage probability, and error probability) [8].

In-order to compensate for the inability to predict of the FSO link's availability,

hybrid FSO/RF systems have emerged as a promising solution for high data rate wireless transmissions [9].

In this thesis, we analyze the performance of Hybrid FSO/RF systems. Hybrid FSO/RF systems have emerged as a promising solution for high data rate wireless transmissions [10]. FSO is a technology that may be used as a stand-alone communications system or in combination with RF systems [11]. In order to compensate for the unpredictability of the FSO link's connectivity, a common a backup RF link can be used in parallel with the FSO link [12].

Previous studies have introduced Hybrid FSO/RF strategies include diversity combining hybrid FSO/RF systems [13], switch over hybrid FSO/RF systems [14], [15], and Hybrid FSO/RF systems with adaptive combining [16], and cross layer analysis of Point-to-Multi-Point $P2MP$ Hybrid FSO/RF network [17].

From another perspective, Hybrid FSO/RF uses the extremely high FSO transmission rates for multi user scenarios to support Point to Multi Point (P2MP) networks [18]. Further, in ($P2MP$) networks, FSO links are used for data transmission from a central location to multiple users [17].

In this thesis we present and analyze a P2MP Hybrid FSO/RF network that uses a number of FSO links for data transmission from the central node to different remote nodes of the network. When more than one FSO link fail, the central node uses a shared backup RF link to transmit a frame to a remote node using an equal priority protocol. Thus, the remote nodes have the same priorities in being assigned the RF link. We assume two traffic classes, high-priority and low-priority classes. The base station reserves two transmit buffers for each user for the down link transmission.

Considering the down link traffic from the base station to a tagged remote node, we study several performance metrics. We develop a cross-layer Markov chain model to study the throughput from central node to a remote node as well as the performance of the resulting system.

1.2 Motivation for this Thesis

The ever growing demand of wireless bandwidth along with huge wireless applications has led to restriction of radio frequency (RF) resources. Free space optical (FSO) transmission systems have considered a promising solution to this limitation [17].

FSO is a wide bandwidth access technique for high data rate applications. As compared to existing RF based wireless systems, FSO is not only cost-effective, but also offers high bandwidth, license-free band use, and causes no interference with existing RF communications systems, because the optical spectrum is a totally different part of the electromagnetic spectrum [19]. However, FSO suffers a critical a drawbacks as well, and it requires a line of sight (LOS) transmission between the transmitter and the receiver. Further, The FSO link is sensitive to atmospheric turbulence which severely degrades the performance of FSO links, while the RF link is more strong to such affected. Hence, these challenges promote the creation of hybrid FSO/RF communication systems. These behaviors of FSO and RF links have led to several studies about hybrid FSO/RF point-to-point system. However, FSO technology can also be used effectively in multi user scenarios [5] to support point-to-multi-point ($P2MP$) topologies.

$P2MP$ topology is a common network architecture for outdoor wireless networks to connect multiple locations to one single central location.

In this thesis, we present a detailed analyses of hybrid point-to-multi-point FSO/RF wireless system. When more than one FSO link fail, the central node will use the RF link to enhance the performance. It will communicate with one of the corresponding remote nodes on an equal priority basis.

1.3 Research Methodology

There are in common two approaches to estimate the performance of hybrid FSO/RF systems with various proposed transmission schemes under the effects of fading and path losses in FSO and RF links. One approach is to conduct experiments, which are usually costly and time exhaustion.

On the other hand, analytical system performance evaluation can be perfect substitutional to experiments, and the gained numerical results can be used efficiently at the beginning stage of system design.

In this thesis, we will focus on efficient analytical performance evaluation of the proposed hybrid FSO/RF network presented, which will equip significant engineering insights into hybrid FSO/RF systems design.

1.4 Contribution

The contributions of this work can be summarized as follow:

1. An-equal priority protocol of P2MP hybrid FSO/RF network for down link traffic is proposed.

2. A Markov chain model of the proposed network is developed.

3. The proposed protocol is modeled using the Monte Carlo method and Several performance metrics are studied.

1.5 Thesis Organization

This section presents a short description of five chapters. A summary of each chapter and its contributions are presented as follows:

Chapter 1, presents the problem considered, scope of the research, the motivation, the objective, and the contributions of the dissertation.

Chapter 2, reviews the basic background and fundamentals of FSO and RF systems. A review of different types of FSO systems and discuss the limitation for these systems. Further, Hybrid FSO/RF presented as an attractive solution for shortcomings of these systems. A brief of this work is presented, Hybrid P2MP FSO/RF network.

Chapter 3, presents and analyzes the P2MP hybrid FSO/RF transmission system in detail. FSO links used to transmit data from the base station to the different remote nodes. The base station will keep two transmit buffers for each node. One buffer is for class-1 traffic and the other is for class-2 traffic. A single-arrival, single departure queuing model is used for each transmit buffer. A different performance metrics are defined such as the throughput, average transmit buffer size, queuing delay, efficiency and the frame loss probability. For comparison purposes, we compare our P2MP hybrid network with the results from previous work.

Chapter 4, presents the parameters of our model to evaluate the performance of the proposed P2MP hybrid FSO/RF in analytical simulation. Introduces the Monte Carlo method for numeric simulation. The simulation results are discussed. For comparison purposes, we compare our P2MP hybrid network with the results from previous work. The comparison includes all the performance metrics with that of P2MP hybrid network.

Chapter 5, contains conclusion of this thesis, summarizes the dissertation contributions and what was achieved of the proposed work, as well as the future work.

Chapter 2

Background and Literature Review

2.1 Background

The consistent demand for higher data rates in support of the demanding applications has promoted the development of Free Space Optics (FSO) and millimeter wavelength (MMW) radio frequency (RF) communication technologies [19]. RF system is convenient in term of cost but offers lower data rate compared with FSO. FSO is a wide bandwidth access technique for high data rate applications [20].

As compared to existing RF based wireless systems, FSO is not only cost-effective, but also offers high bandwidth, license-free band use, and causes no interference with existing RF communications systems, because the optical spectrum is a totally different part of the electromagnetic spectrum. However, FSO suffers a critical a drawbacks as well, and it requires a line of sight (LOS) transmission between the transmitter and the receiver. Further, The FSO link is sensitive to atmospheric turbulence which severely degrades the performance of FSO links, while the RF link is more strong to such affected [19].

A solution to this issue is to combine FSO and RF links. Millimeter wave RF systems, achieve data rates equal with FSO systems. These behaviors of FSO and RF links have led to several studies about hybrid FSO/RF point-to-point system. However, FSO technology can also be used effectively in multi user scenarios to support point-to-multi point (P2MP) topologies [5].

2.2 Literature Review

2.2.1 Free-Space Optical Communications

Free space optical (FSO) technology has earned high attention in implementing point-to-point data transmission links, due to its high bandwidth, low cost implementation in a non-licensed spectrum, and high transmission security compared with RF technology, it also provides a cost-effective optical wireless connectivity and a faster deployment unlike fiber optics. FSO technology has evolved to its current stage for deployment in many applications due recent developments and market acceptance of FSO links [21].

FSO systems slowly gained acceptance in the marketplace as a solution to change expensive optical fibers [22]. FSO provides relatively right bandwidth for point-to-point communication as last mile applications and also for indoor communication, and many features such as spatial reuse, usage of low-power per bit transmitted, licensed-free band, and higher bandwidth [23].

FSO links can be implemented with optical fibers to connect one (LAN) to another (LAN) and connect them to Backbone networks. The black arrows in Figure 2.1 represent FSO links [1].

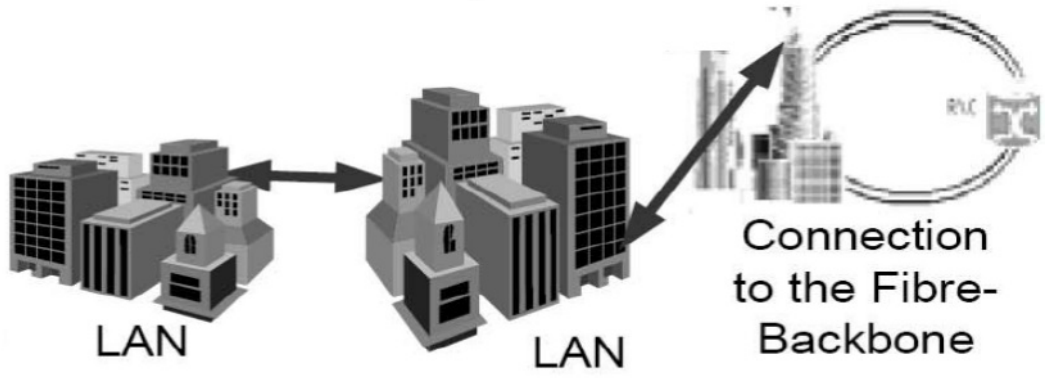

Figure 2.1: LAN-to-LAN FSO connectivity [1].

FSO links can be used also as a robust outdoor backhaul solution for small radio cells, such as $WiFi$, LTE and $5G$ as shown in Figure 2.2 [2].

Moreover, FSO links can be used in point-to-point links, and in point-to-multi-point links [24], in last mile access [25], and In storage area network SAN [25].

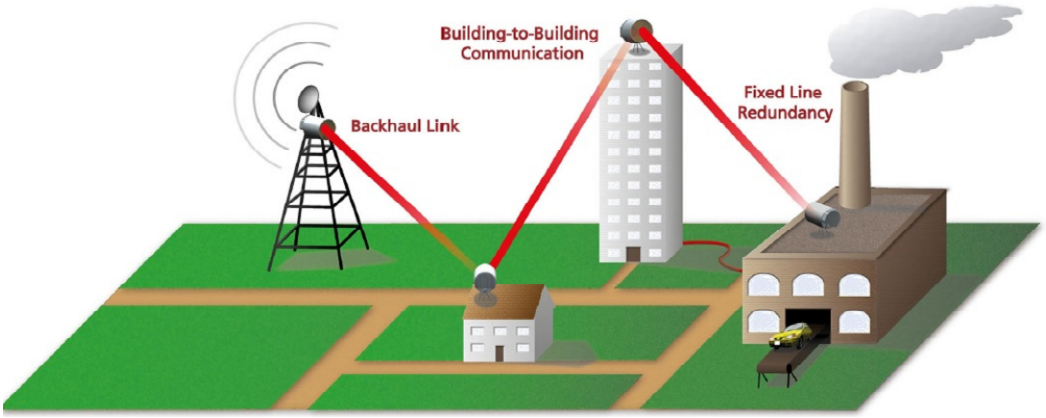

Figure 2.2: Point-to-point backhaul FSO link [2].

The FSO system block diagram is given in Figure 2.3. It consists of three main blocks an optical transmitter, channel, and an optical receiver. FSO systems can be based on the intensity modulation with direct detection (IM/DD) coherent scheme [26].

The FSO technology in general depends on the propagation of the laser beam through the atmosphere, in which the optical signal is affected by several factors including the atmospheric loss, due to the visibility affected by particles such as rain, snow, fog, dust, smoke. Causing an reduction of the optical power, and light scattering [27]. The FSO systems are deployed in metropolitan areas.

Moreover, Misalignment Loss mostly occurs because of in homogeneities of wide-scale atmosphere eddies that led to random deflections of the optical beam [28]. The optical signal launched from the transmitter is affected by fading before arriving at the receiver due to atmospheric turbulence and pointing errors [29], [30] as shown in Figure 2.4 [3], this changes known as the scintillation or fading.

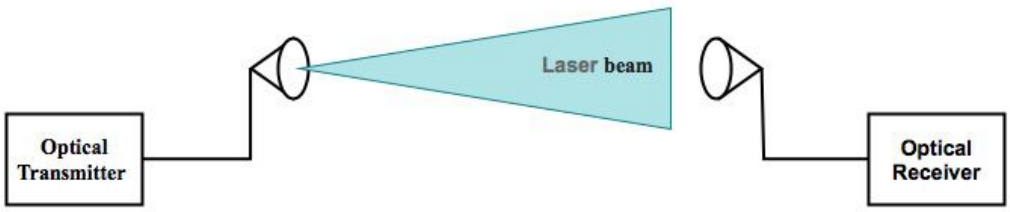

Figure 2.3: FSO system block diagram.

These fluctuations can increase the probability of error and impair the performance of FSO system, especially in long distance communications [31].

2.2.2 Hybrid FSO/RF Implementation

According to the different propagation properties of RF and FSO systems, it is possible to utilize these two technologies assist one another. Despite the fact that optical signal is highly affected by weather states, the integrating of the FSO link with a Millie-Meter wavelength (MMW) RF link will improve the performance of FSO links and link availability.

In fact, there is roughly endless number of weather conditions which have either positive or negative impact on RF and FSO link, respectively. However, FSO and RF links are affected fully differently by atmospheric and weather conditions. In the sense that the FSO links is severely affected by fog, whereas the RF signal is not and the MMW RF links is severely affected by rain, whereas FSO links is not. Thus, when the FSO link fails, the other link of the hybrid FSO/RF system is complementary to each other to maintain reliable communication at a reduced data rate [32].

Likewise, the atmospheric turbulence causes a small scale fading in FSO links [5], while RF links are harmed by fading through multi-path propagation [33]. Real hybridization is achieved through both channels when reparation the shortcomings of one another and thereby increase performance the system as a whole.

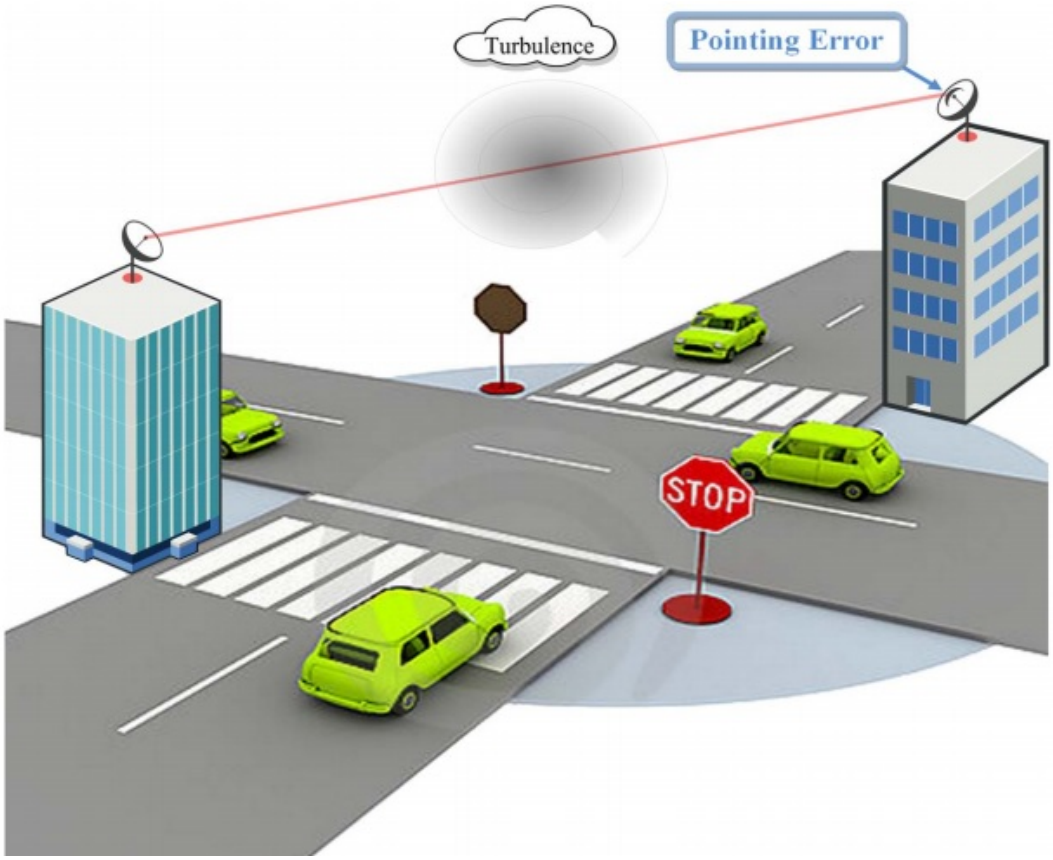

Figure 2.4: Atmospheric turbulence and pointing error in FSO system [3].

Hybrid network, a combination of FSO major link and radio frequency back up link, is a practical solution to overcome the atmospheric attenuation. The selection of the frequency for the backup link in a hybrid FSO/RF system require the study of different link attenuates severally as a solution which assures great availability under different operating weather status.

Besides the several approaches of implement hybrid FSO/RF systems, the complementary perform of FSO and MMW RF links has led to two prime approaches of implementing hybrid FSO/RF systems [34].

Thus, different approaches to switching between the RF and the FSO links have been proposed in the literature. In [15], the hardware switching scheme is proposed one activated link of transmit data switched from optical to RF when the optical link degrades. This scheme requires frequent hardware switching between both the RF and the optical links. Therefore, a soft switching is proposed as an alternate scheme, in which both links are active with one another [35], [36].

Two methods are presented depending of this scheme. One method is when same data with identical data rate is transmitted over both links [35]. The main drawback is an extreme data rate limited by the RF link and the high data rate optical link is never used efficiently.

Another method is most of the data is transmitted over the optical link and only a small fraction of data is sent over the RF link [36]. In this method, RF transmission is activated despite of the FSO link keeps the predefined QoS. This causes in wastage of RF power and RF interference. These drawbacks of the above approaches led to proposed a combination to overcome these issues, a new scheme was discussed in [9].

The FSO link is utilized alone for transmit data provided that its quality of (SNR) is more than a threshold and the RF link is put on standby mode. When the FSO link deteriorates, the system uses the RF link, and both using for sent same data with same data rate.

At the receiver, the maximal ratio combining (MRC) is utilized to restore the main data. While keeping the RF link is on standby mode as long as the FSO link is acceptable. Therefore, the adaptive combining scheme for hybrid FSO/RF systems improves the reliability of system communication, averts generation of undue RF interference, keeps RF power, and utilizes from FSO higher data rate exceedingly [14].

In [37], a hybrid MIMO FSO/RF system with optical space shift keying ($OSSK$) employed at FSO subsystem has proposed to increase the throughput and reliability of the system. The FSO channel is modeled as Malaga distributed and RF channel

is assumed to be Nakagami distributed. Spatial modulation (SM) at the transmitter is incorporated to increase the spectral efficiency and selection combiner is employed at the receiver to achieve higher diversity order.

The authors in [38] evaluated the performance of relay selection in an energy harvesting aided mixed RF/FSO system over atmospheric turbulence and pointing error. Where transmit antenna selection and (SC) diversity scheme are respectively used by source to transmit information to destination and harvest energy from the relay node. The results illustrate that the atmospheric turbulence and (NB) pointing error strongly degrade the system performance. Moreover, the increase in the number of source antennas as well as relay nodes significantly improves the system performance.

Likewise, strong turbulent conditions besides high pointing error increases the dependence on the RF resource, thereby, increasing the RF usage more efficiently. In [39] the authors presented the possibility of sharing a RF resource between two FSO links on a cognitive basis, thus, forming a cognitive Hybrid FSO/RF link along with the existing Hybrid FSO/RF link. A second FSO link is converted to a cognitive Hybrid FSO/RF link by accessing the already existing RF in the cognitive interweave mode, the results indicate improved system performance and better overall utilization of the RF resource.

2.2.3 Point-to-Multi-Point Transmission

By investing a range of advantages, P2MP topology at multi-user scenarios will open new conception for future outdoor wireless networks. On the one hand, P2MP approach can compound link utilization then realizing higher transmission, compared to point-to-point data transmission (P2P). However, P2MP technique needs much minimal cost for an one link than the P2P technique [40].

In the literatures, FSO technology has been used effectively in multi-user scenarios, such as [41] and [42] supported Point-to-Multi-Point (P2MP) topologies.

P2MP topology is a shared network architecture for outdoor wireless networks to connect multiple users to a single central location, as shown in Figure 2.5 [4].

In [43], the FSO links in P2MP networks, have been used for transmitting data from a central location to multiple users as in Wireless Internet Service Provider (WISP) networks or the WiMAX networks. Likewise, in WISP network, the multiple locations are connected by the network using a client device. The central location is mounted on a high location where it has line of sight with the user devices.

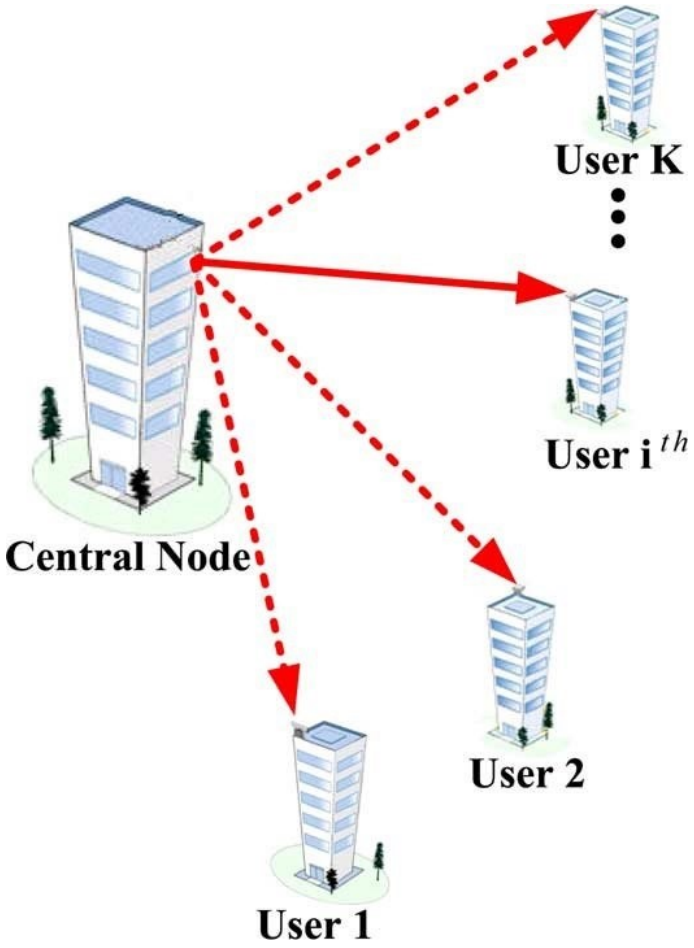

Figure 2.5: Point-to-multi-point FSO communication system [4].

Due to the scarcity of the literature and the minimal number of studies covering this field, we propose a P2MP hybrid FSO/RF network. The proposed P2MP hybrid FSO/RF data transmission network consists of a number of remote nodes along with a central node. Every single remote node in the network is connected to the central node through a autonomous initial FSO link. The central node use a shared backup RF link for data transmission to any user in case of the failure of its FSO link. Thus, using a common RF channel will provide many advantages such as, sharing the rare RF spectrum, preventing the generation of unneeded RF interference, and keeping the RF transmitting power.

2.3 Summary

In this chapter, we have review the basic background and fundamentals of FSO and RF systems and its application in previous literatures.

Further, we discussed the shortcomings of FSO point-to-point (P2P) technology and its applications.

Moreover, a review of different types of FSO systems and discuss the limitation for these systems.

Lastly, Hybrid FSO/RF presented as an attractive solution for shortcomings of these systems. A brief of this work is presented, Hybrid P2MP FSO/RF network. The following chapter describes our Hybrid P2MP FSO/RF network in detail with its performance metrics.

Chapter 3

Analysis of Point-to-Multi-Point Hybrid FSO/RF Network

In this chapter, we analyze a P2MP hybrid FSO/RF data transmission network. This network consists of a central node with N remote nodes. The central node is provided with N optical transmitters and one RF transmitter. Each one of the remote nodes receive data from the central node through a separate primary FSO link. The central node is assigned a common backup RF link, which is used as a backup channel for data transmission to any remote node in case of the failure of its corresponding FSO link. Using a common RF channel will have the main advantages such as sharing the scarce RF spectrum, preventing the generation of unnecessary RF interference to the environment, and conserving the RF power. We study the performance of only one of the remote node (tagged node) instead of studying all system performance. Examining the tagged node grant us to investigate several performance criteria such as throughput from central node to the tagged node, the frame queuing delay in the transmit buffer , the average transmit buffer size, the frame loss probability, the efficiency of the queuing system are determined for the proposed FSO/RF topology.

3.1 P2MP network FSO/RF Network Modeling

The general block diagram of a P2MP hybrid FSO/RF network is shown in Fig. 3.1. This network is formed of a central node and N remote nodes. The central node is

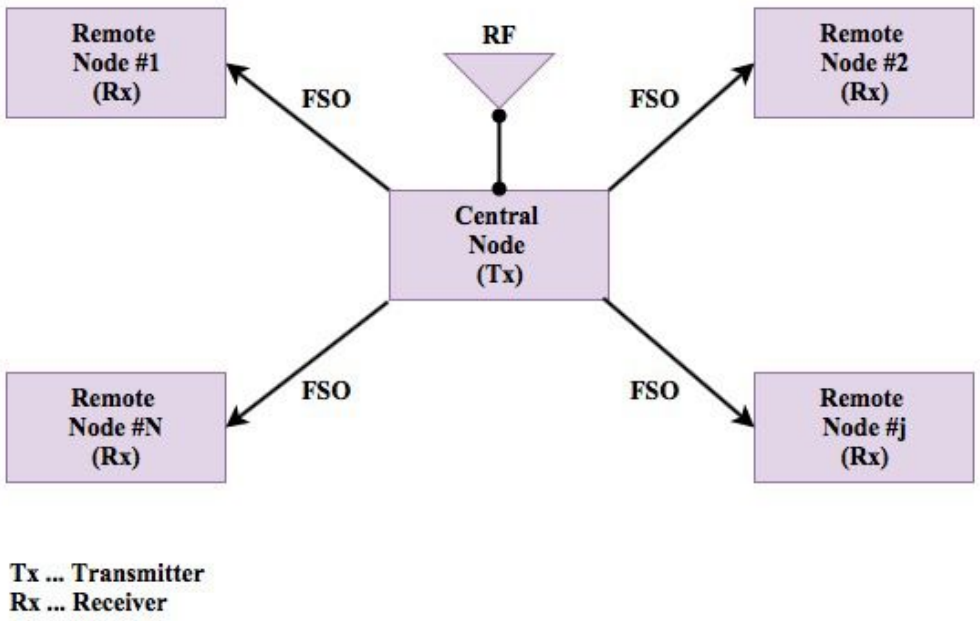

Figure 3.1: General block diagram of a P2MP Hybrid FSO/RF network.

provided with N optical transmitters and one RF transmitter. Each one of the remote nodes receive data from the central node through a separate primary FSO link. The central node is assumed to be aware of the quality of the N FSO links through N feedback channels. The RF transmitter of the central node is assigned a certain RF channel, which is used as a backup channel for data transmission to any remote node in case of the failure of its corresponding FSO link. The central node is assigned a common backup RF link, which is used as a backup channel for data transmission to any remote node in case of the failure of its corresponding FSO link.

We will model here the down link traffic from the base station to the users. In order to start the analysis we make the following system-level assumptions:

1. There are two traffic classes: high-priority class-1 traffic and low-priority class-2 traffic.

2. There are N equal priority users.

3. The base station reserves two transmit buffers for each user: B_1 and B_2 for class-1 and class-2 traffic, respectively.

4. The base station chooses class-1 traffic with probability p and chooses class-2 traffic with probability $1 - p$.

5. The data frame arrives with probability w_1 for class-1 traffic and w_2 for class-2 traffic.

6. Probability FSO link is bad is given by a and probability that RF link is bad is given by b.

7. We choose the time step T to allows a single-arrival, single-departure queue.

From the above assumptions we have two $M/M/1/B$ queues for the two buffers of each user.

Table 3.1: Comparison of the existing P2MP network and previously mentioned networks.

The Comparison Of P2MP Networks				
P2MP Network Presented By	Traffic Classes	Node Classes	P-Persistent Strategy	RF and FSO Rate
A. Boharba	✓	X	X	An-equal rates
Y.A. Ansari	X	✓	✓	Non-equal rates
N. Lashari	X	✓	X	X
T. Rakia	X	X	X	X

Table 3.1 illustrates the comparison of the existing P2MP network and previously networks presented in [17], [44] and [45].

The results of this existing P2MP network are also compared with an efficient P2MP networks presented in [17], [44] and [45].

For the analyses of a P2MP networks, there are many existing networks in the literature. As an example, a new P2MP network based on hybrid FSO/RF transmission

system is presented by T. Rakia to achieve considerable performance improvement of P2MP Hybrid FSO/RF network over the P2MP FSO-only network [17]. This network is based on a cross layer Markov chain model and the data is transmitted over the FSO and RF links at the same rate subject to a number of constraints. Further, an equal priority protocol when transmitting to a remote node using a common backup RF link, where the lowest number node will have the highest priority as summarized in Table 3.1. As a result, the network performance yields a small limitation.

Another P2MP network is present a new model that introduced in [44]. This P2MP network presents a new analyses based on a cross layer Markov chain model to improve the performance metrics of previous network. A non-equal priority protocol is introduced when transmitting to a remote node using a common backup RF link, where first node has the highest priority for accessing the RF link as in Table 3.1. As a result, the network performance suffers a small constraints.

Another recent P2MP network is present a new strategy that projected in [45]. This network deploy a non-equal priority protocol and p-persistent strategy for nodes accessing the RF link and consider the back up RF transmission link with lower frame transmission rates as compared to the FSO link. Using p-persistent strategy on non-equal priority basis, where the lowest number node will have the highest priority as shown in Table 3.1. This P2MP network improves the performance metrics of previous networks.

Unlike the P2MP network presented in Chapter 3, the two mentioned networks in [44] and [45] use non-equal priority protocol, where the lowest number node will have the highest priority and the data frame is transmitted over the FSO and RF links at different rates [45]. While P2MP network mentioned in [17] use an equal priority protocol, where the lowest number node will have the highest priority and the resulting Markov chain is a single-arrival, single-departure queue.

In this P2MP network, FSO links are used for data transmission from a central location to multiple users. When more than one FSO link fail, the central node uses a common backup RF link to transmit a frame to a remote node using an equal priority protocol. We assume two traffic classes, a high-priority and low-priority classes. The base station reserves two transmit buffers of each user for the down link transmission as summarized in Table 3.1. Considering the down link traffic from the base station to a tagged remote node, we study several performance metrics. We develop a cross-layer Markov chain model to study the throughput from central node to a remote node as well as the performance of the resulting system.

3.2 FSO and RF Channel States

The FSO link is the main channel used for data transmission as long as the instantaneous signal-to-noise ratio (SNR) at the optical receiver of the remote node is above a certain threshold. When SNR falls below the certain threshold, the central node uses the RF link for data transmission.

We define a to be the probability that a certain FSO link is in poor quality. The actual calculations of a are defined in [1, 9, 17].

Similarly, the RF link is also affected by fading and we define b to be the probability that the RF link is in poor quality due to fading and can not be used for data transmission. The actual calculations for b are defined in [1, 9, 17].

3.3 An Equal Priority Protocol

Since we allocated only one backup RF link, the central node uses the common RF link to communicate with any one of the remote nodes with failed FSO links on an-equal priority basis.

An equal priority protocol means that the remote nodes have equal priorities in being assigned the RF link. The base station reserves two transmit buffers for class-1 and class-2 traffic for each user. Class-1 traffic is considered the highest-priority traffic and class-2 traffic is the lowest-priority traffic.

With failed FSO link, when using equal priority protocol to serve all the remote nodes, the central node will use the common backup RF link to send data frame with probability p for class-1 traffic with the highest priority.

3.4 Steady State System Performance Modeling

Since all the remote nodes are identical, we can study the system performance by focusing on one remote node (tagged node).

3.4.1 Private Communications of Channel Access Probability with Dr.Fayez Gebali [24].

In this section we will find expression for the probability a tagged node getting access to the FSO or RF channels.

The tagged node does not compete if the FSO channel is available with probability $1-a$.

To find the probability that the tagged node gets access to the RF channel we need to consider the state of the other nodes. Assuming the tagged node has bad FSO channel but its RF channel is available, we define x_a to be the probability that a user requires the RF channel.

The probability that a user requires the RF channel is given by three independent events:

1. FSO channel is bad
2. RF channel good
3. There is at least one frame from class-1 traffic or class-2 traffic

This is expressed as:

$$x_a = a(1-b)\left[w_1 s_1(0) + (1-s_1(0)) + w_2 s_2(0) + (1-s_2(0))\right] \tag{3.1}$$

where $s_1(0)$ and $s_2(0)$ are the probabilities that class-1 or class-2 buffers are empty, respectively.

Assuming the tagged node requires the RF channel, the probability that it is granted access to the RF channel is given by:

$$\begin{aligned} x_{RF} &= \binom{N-1}{0} x_a^0 (1-x_a)^{N-1} + \frac{1}{2}\binom{N-1}{1} x_a^1 (1-x_a)^{N-2} \\ &\quad + \frac{1}{3}\binom{N-1}{2} x_a^2 (1-x_a)^{N-3} + \cdots + \frac{1}{N}\binom{N-1}{N-1} x_a^{N-1} \qquad (3.2) \\ & \qquad (3.3) \\ &= \sum_{i=0}^{N-1} \frac{1}{i+1}\binom{N-1}{i} x_a^i (1-x_a)^{N-i-1} \qquad (3.4) \end{aligned}$$

The probability that the tagged user gets access to a channel is given by

$$p_{ch} = (1-a) + a(1-b)x_{RF}$$

3.4.2 Probability of Channel Access for Each Traffic Class

Independent of the state of the FSO or RF channels, we need to find probabilities of selecting traffic from Class-1 or Class-2.

Assuming that Class-1 traffic requires access to the channel, the probability that it is selected is given by:

$$y_1 = (1 - w_2)s_2(0) + [w_2 s_2(0) + 1 - s_2(0)]\, p \tag{3.5}$$

Similarly, the probability that class-2 buffer is selected, when it requires channel access, is given by:

$$y_2 = (1 - w_1)s_1(0) + [w_1 s_1(0) + 1 - s_1(0)]\, (1 - p) \tag{3.6}$$

where $s_1(0)$ and $s_2(0)$ are the probabilities that class-1 buffer is empty or class-2 buffer is empty, respectively.

Having found p_{ch}, y_1 and y_2, we now need to know the probability of selecting a packet from each buffer. The probability that the tagged user Class-1 buffer is able to transmit on the FSO/RF channel is given by:

$$z_1 = p_{ch}\ y_1 \tag{3.7}$$

Likewise, the probability that tagged user Class-2 traffic accesses the FSO/RF channel is given by:

$$z_2 = p_{ch}\ y_2 \tag{3.8}$$

3.4.3 Tagged Node Queuing Model

The central node assigns a first-in-first-out (FIFO) transmit buffer of size B frames for every remote node. The data frames arrive at the transmit buffer at rate R_{in} frames/second. The frame arrival rate R_{in} is assumed to be the same for all the N transmit buffers. We define R_{out} as the frame departure rate. To prevent transmit buffer overflow, we must ensure that R_{out} is greater than or equal to R_{in}. Here, the frame arrival rate R_{in} changes over time with maximum value equal to R_{out}. We can use the discrete-time Markov chain to model the states of the transmit buffer for the tagged node. The time step of the discrete-time Markov chain, denoted by T, is

chosen as:

$$T = \frac{1}{\max(R_{in}, R_{out})} \tag{3.9}$$

We choose the time step T to allows a single-arrival, single-departure queue.

$$\begin{aligned} T &> T_1 && (3.10)\\ T &< \min(T_1, T_2) && (3.11)\\ &< \frac{1}{\max(R_{in}, R_{out})} && (3.12) \end{aligned}$$

Figure 3.2 shows the state transition diagram for the class-1 or class-2 buffers, where it was assumed that each buffer is of size B. The probabilities in the figure for

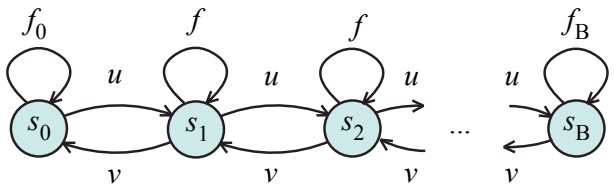

Figure 3.2: State transition diagram for class-1 or class-2 buffers.

class-1 buffer are given by:

$$\begin{aligned} f_1(0) &= (1 - w_1) + w_1 z_1 && (3.13)\\ u_1 &= w_1(1 - z_1) = 1 - f_1(0) && (3.14)\\ v_1 &= (1 - w_1) z_1 && (3.15)\\ f_1 &= 1 - u_1 - v_1 && (3.16)\\ f_1(B) &= 1 - v_1 && (3.17) \end{aligned}$$

For class-2 traffic, Fig. 3.2 still applies but the transition probabilities are given by:

$$\begin{aligned} f_2(0) &= (1 - w_2) + w_2 z_2 && (3.18)\\ u_2 &= w_2(1 - z_2) = 1 - f_2(0) && (3.19)\\ v_2 &= (1 - w_2) z_2 && (3.20)\\ f_2 &= 1 - u_2 - v_2 && (3.21)\\ f_2(B) &= 1 - v_2 && (3.22) \end{aligned}$$

The state transition matrix $\mathbf{P}$ for either class-1 or class-2 traffic is given by:

$$\mathbf{P} = \begin{bmatrix} f_0 & v & 0 & \cdots & 0 & 0 & 0 \\ u & f & v & \cdots & 0 & 0 & 0 \\ 0 & u & f & \cdots & 0 & 0 & 0 \\ \vdots & \vdots & \vdots & \ddots & \vdots & \vdots & \vdots \\ 0 & 0 & 0 & \cdots & f & v & 0 \\ 0 & & 0 & \cdots & u & f & v \\ 0 & & 0 & \cdots & 0 & u & f_B \end{bmatrix} \tag{3.23}$$

The steady state distribution vector $\mathbf{s}$ corresponding to Fig. 3.2 or Eq. (3.23) is given by:

$$\mathbf{s} = [\ s_0 \quad s_1 \quad \cdots \quad s_B\ ]^t \tag{3.24}$$

where s_i is the probability that the transmit buffer has i frames, where $0 \leq i \leq B$.

According to [24], the distribution vector components must satisfy the normalization condition:

$$\sum_{i=0}^{B} s_i = 1 \tag{3.25}$$

At steady state, the distribution vector $\mathbf{s}$ satisfies the equation:

$$\mathbf{P}\ \mathbf{s} = \mathbf{s} \tag{3.26}$$

The steady-state distribution vector $\mathbf{s}$ is the eigenvector of $\mathbf{P}$ that corresponds to unity eigenvalue. From Eq. 3.26, we can write the following set of difference equations:

$$-us_0 + vs_1 = 0 \tag{3.27}$$

$$us_0 - (v+u)s_1 + vs_2 = 0 \tag{3.28}$$

$$us_{i-1} - vs_i - (u+v)s_i + vs_{i+1} = 0; \quad 0 < i < B \tag{3.29}$$

The solution of the above set of difference equations can be given in general form as [24]:

$$s_i = \rho^i s_0, \qquad 0 \leq i \leq B \tag{3.30}$$

where for class-1 traffic $\rho 1$ is given by:

$$\rho 1 = \frac{u1}{v1} = \frac{w_1(1-z_1)}{(1-w_1)z_1} \tag{3.31}$$

and for class-2 traffic, $\rho 2$ is given by:

$$\rho 2 = \frac{u2}{v2} = \frac{w_2(1-z_2)}{(1-w_2)z_2} \tag{3.32}$$

The solution for s_0 obtained by substituting (3.30) in (3.25) gives:

$$s_0 = \frac{1-\rho}{1-\rho^{B+1}} \tag{3.33}$$

Combining (3.33) and (3.30) gives the states as:

$$s_i = \frac{(1-\rho)\rho^i}{1-\rho^{B+1}} \quad , \quad 0 \leq i \leq B \tag{3.34}$$

3.5 Tagged Node Performance Metrics

The steady state distribution vector $\mathbf{s}$ allows us to analyze the various performance metrics as explained in the following subsections.

3.5.1 Throughput from Central Node to the Tagged Node

We define the throughput Th as the probability of transmitting a frame over a frame period. The Th_1 for class-1 traffic can be calculated as:

$$Th_1 = [w_1 s_0 + (1 - s_0)]\, z_1 \tag{3.35}$$

where the first term on the RHS is the probability a frame leaves the buffer when the buffer is empty. The second term on the RHS is the probability a frame leaves the buffer when it is not empty. Using (3.25), the expression in (3.35) becomes:

$$Th_1 = z_1\,[1 - s_0(1 - w_1)] \tag{3.36}$$

Likewise, the throughput Th_2 of class-2 traffic is given by:

$$Th_2 = z_2 \left[1 - s_0(1 - w_2)\right] \tag{3.37}$$

3.5.2 Average Buffer Size

The average buffer size Q_a is the average number of frames in the buffer, which can be expressed as:

$$Q_a = \sum_{i=0}^{B} i s_i \tag{3.38}$$

This expression represents the weighted sum of the number of frames in the buffer. Substituting (3.30) in (3.38) and using [[24], Eq (1.2.2.3)] the the average buffer size is given by:

$$Q_a = \frac{\rho[1 - (B+1)\rho^B + B\rho^{B+1}]}{(1-\rho)(1-\rho^{B+1})} \tag{3.39}$$

3.5.3 Average Buffer Queuing Delay

The average queuing delay T_q is the average number of time steps that a frame spends in the buffer before being transmitted. Using Little's result, this delay is given by [24]:

$$T_q = \frac{Q_a}{Th} \tag{3.40}$$

3.5.4 Frame Loss Probability

A frame is lost in the queue when it arrives to a full transmit buffer and a head symbol is not able to leave the queue. Using traffic principle described in [24], the frame loss probability P_L is given by:

$$P_L = w s_B (1 - (z_{1,2})) \tag{3.41}$$

3.5.5 Efficiency of the Queue

The ratio of probability of a frame leaving the buffer relative to the probability that a frame arriving at the buffer, denoted by φ , is expressed as:

$$\varphi = \frac{Th}{w} = \frac{(z_{1,2})\left[1 - s_0(1 - (w_{1,2})\right]}{w} \tag{3.42}$$

The efficiency φ gives an indication of frame loss due to buffer overflow. A value of $\varphi = 1$ implies no buffer overflow. A value of $\varphi < 1$ implies buffer overflow and potential frame loss.

3.6 Summary

In this chapter, we defined a P2MP network based on hybrid FSO/RF transmission system. In case its fail FSO link, A common backup RF link is used to transmit data from the central node to the tagged node. We studied the performance of a tagged node instead of studying all system performance. A Cross layer Markov chain model was developed for the transmit buffer of the link among the central node and the tagged remote node on an equal priority basis. We presented a various performance metrics based on a single remote node (tagged node) such as throughput from central node to the tagged node, the average transmit buffer size, the frame queuing delay in the transmit buffer, the efficiency of the queuing system, and frame loss probability

Chapter 4

Analytical and Numerical Results

In this chapter, we present several analytical and numerical results to clarify the analysis introduced in Chapter 3. We developed a MATLAB code to study the performance evaluation of the defined network.

In Section 4.1, we discuss the relevant parameters of the FSO and RF considered for the numerical results given in Table 4.1, and provided the required values to calculate the performance of proposed network.

In Other Sections, we illustrate different graphs of the existing P2MP network performances and summarized of each at the end.

For comparison purposes, we compare our P2MP hybrid network performance metrics with that of P2MP hybrid network presented in [17], [44] and [45].

The comparison includes throughput from the central node to remote nodes, Average queuing delay, Average buffer size, Frame loss probability and the efficiency of the remote nodes. However, due to the different ways of presenting these results in the other papers, sometimes it is not possible to compare all performance parameters, such as transmitting the data frame over the FSO and RF links at non-equal data rate.

4.1 Parameters of FSO and RF subsystems

FSO and RF links are affected completely differently by atmospheric and weather conditions. Both the FSO and RF links are fading greatly affected by atmospheric conditions which are embedded in for the calculations of a and b in [1]. The FSO link is affected by foggy weather while the RF link affected by rainy weather. Thus, we

only use certain values of a and b representing typical weather conditions to test the model. Further we assume different values of probability p for transmitting over the common backup RF link.

Table 4.1: Parameters of FSO and RF subsystems.

FSO and RF subsystem		
Parameter	frame	Value
Probability of FSO link in poor condition	a	0.1
Arrival probability	ω_1	0.01 - 1.00
Frames arrive with probability for class-2	ω_2	0.25, 0.5
Probability of RF link in poor condition	b	0.9
Total number of nodes	N	4
Transmit buffer size class-1	B_1	6
Transmit buffer size class-2	B_2	6
The probability of chosen class-1 traffic over class-2 traffic	p	0.5, 1

Table 4.1 illustrates the parameter values we will use to evaluate the performance for our Hybrid FSO/RF system.

For comparison purposes, the parameters values of our P2MP network is set to $a = 0.1$, $b = 0.9$, $B = 6$, and p probability value is considered as $p = 1$, $\omega_2 = 0.5$ instead of other existing values because it gives better results. However, the results obtained are still used to evaluate and compare the existing P2MP network results with its counterparts.

There are generally three approaches by which scientific problems and equations are solved, Analytical, Numerical and Experimental. However, we can not perform experimental method every time because of cost and time constraints.

Analytical methods are the conventional methods to solve problems. But due to restraints caused due to complex Geometry, Boundary conditions, etc we are not able to solve equation analytically. Further than this, the method of solution must be easier to become skilled in than the usual methods (i.e. analytical solutions). And the results must be easy to verify much easier than is the case with a complicated piece of algebra.

Moreover, the time required to arrive at the desired result by analytical methods can not be foreseen with any certainty. Many problems exist that have no analytical solution. And even problems with analytical solutions do have them because lots of

constants are assumed to be constant. However the analytical solution to a simplified problem learns us a lot about the behavior of the system. On the other side if no analytical solution method is available then we can investigate problems quite easily with numerical methods. However care has to be taken that a converged solution is obtained.

So, from past many years we are moving towards Numerical methods as they can provide almost accurate result in comparison with analytical method and that too in less time and easy way. Further, numerical method always works with iteration. When we determine the final answer for each question must together with some errors.

Numerical results are presented and validated by Monte Carlo simulations, which follows the same Monte Carlo procedure as described in [46]. Monte Carlo methods are a class of computational algorithms can be applied to wide ranges of problems, and rely on repeated random sampling. This method is used to solve systems that might be deterministic in principle. The analytical results have been verified by using Monte-Carlo simulation.

4.2 Throughput Th Results and Discussion

In this section, we present selected numerical examples to illustrate our analysis introduced in Chapter 3. The results of this existing P2MP network are also compared with an efficient P2MP networks presented in [17], [44] and [45].

4.2.1 Simulation Results

In Fig. 4.1, we plot the throughput Th as function of the frame arrival probability ω_1 for different classes traffic with N equal priority users and equal values of buffer size.

We consider $a = 0.1$, $b = 0.9$, the buffer size of each classes traffic is $B = 6$, and p probability value is considered as $p = 1$. The results obtained from our P2MP network are compared with results using the P2MP network presented in [17], [44], and [45].

It can be seen in Fig.4.1 (a), the throughput graph shows two phases viz linear and saturation. The linear phase occurs at low ω_1 values, while the saturation phase occurs for higher values of ω_1. The transition point occurs when the frame arrival probability $\omega_1 = 0.9$. Since we have used an equal priority protocol, the tagged

node does not compete if the FSO channel is available. Class-1 shows the highest throughput because it has the highest priority of accessing the RF link. On the other hand, Class-2 has the lowest priority of accessing the RF link, so it shows the lowest throughput.

For Class-1, the transition from linear to saturation phase occurs when the transmit buffer is not empty. The throughput for Class-1 saturates at $Th = 0.9$ because the RF link is being accessed with the probability p and there is no dip in throughput because of an equal priority protocol.

The Class-2 starts and remains saturated at $Th = 0.5$ with probability FSO and available RF link. The throughput for Class-2 saturates at $Th \neq 0$ because of p probability; the tagged node does not compete if the FSO channel is available. The decreasing throughput occurs for higher values of ω_1. Class-2 traffic transition points in throughput occur at region $\omega \in [0.45, 1]$ with decreasing throughput $Th = 0.45$. This is because the RF link access priority increase with decreases in priority of classes.

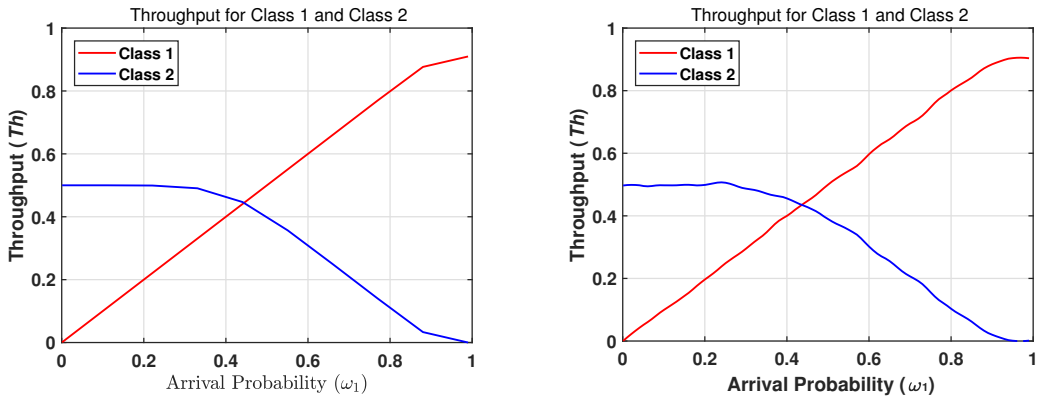

Figure 4.1: Throughput with a = 0.1, b = 0.9, p = 1, $\omega_2 = 0.5$, $B_1 = 6$, and $B_2 = 6$ frames. (a) Analytical simulation. (b) Numerical simulation.

Fig.4.1 (b) shows Monte Carlo simulation for the same parameters and results shows strong agreement with the analytical model.

In Fig. 4.2, we plot the throughput Th as function of the frame arrival probability ω_1 for different classes traffic with N equal priority users and equal values of buffer size.

We consider $a = 0.1$, $b = 0.9$, the buffer size of each classes traffic is $B = 6$, and p probability value is considered as $p = 0.5$.

It can be seen in Fig.4.2 (a), the throughput graph shows two phases viz linear and saturation. The linear phase occurs at low ω values, while the saturation phase occurs for higher values of ω_1. The transition point occurs when the frame arrival probability $\omega_1 = 0.45$. Class-1 shows the highest throughput because it has the highest priority of accessing the RF link. On the other hand, Class-2 has the lowest priority of accessing the RF link, so it shows the lowest throughput.

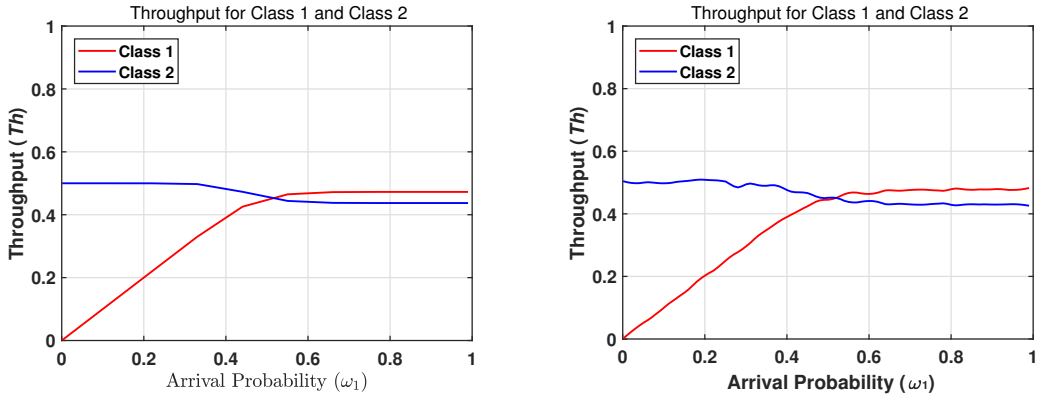

(a) (b)

Figure 4.2: Throughput with a = 0.1, b = 0.9, p = 0.5, $\omega_2 = 0.5$, $B_1 = 6$, and $B_2 = 6$ frames. (a) Analytical simulation. (b) Numerical simulation.

For Class-1, the transition from linear to saturation phase occurs when the transmit buffer is not empty. The throughput for Class-1 saturates at $Th = 0.43$ because the RF link is accessed with the probability p and there is no dip in throughput.

The Class-2 starts and remains saturated at $Th = 0.5$ with probability FSO and available RF link. The throughput for Class-2 saturates at $Th \neq 0$ because of p probability; the tagged node does not compete if the FSO channel is available and no dip in throughput because of an equal priority protocol.

Fig.4.2 (b) shows Monte Carlo simulation for the same parameters and results shows strong agreement with the analytical model.

In Fig. 4.3, we plot the throughput Th as function of the frame arrival probability ω_1 for different classes traffic with N equal priority users and equal values of buffer size.

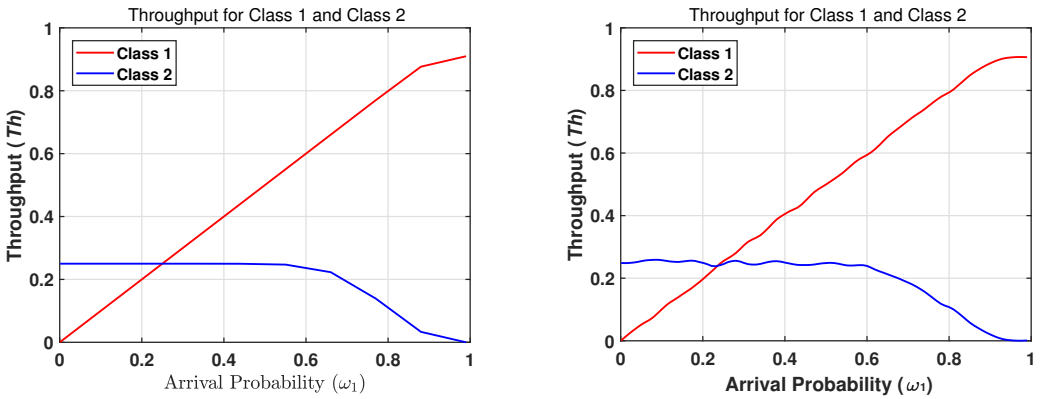

Figure 4.3: Throughput with a = 0.1, b = 0.9, p = 1, $\omega_2 = 0.25$, $B_1 = 6$, and $B_2 = 6$ frames. (a) Analytical simulation. (b) Numerical simulation.

We consider $a = 0.1$, $b = 0.9$, the buffer size of each classes traffic is $B = 6$, and p probability value is considered as $p = 1$.

It can be seen in Fig.4.3 (a), the throughput graph shows two phases viz linear and saturation. The linear phase occurs at low ω_1 values, while the saturation phase occurs for higher values of ω_1. The transition point occurs when the frame arrival probability $\omega_1 = 0.85$. Class-1 shows the highest throughput because it has the highest priority of accessing the RF link. On the other hand, Class-2 has the lowest priority of accessing the RF link, so it shows the lowest throughput.

For Class-1, the transition from linear to saturation phase occurs when the transmit buffer is not empty. The throughput for Class-1 saturates at $Th = 0.9$ because the RF link is being accessed with the probability p and there is no dip in throughput because of an equal priority protocol.

The Class-2 starts and remains saturated at $Th = 0.25$ with probability FSO and available RF link. The throughput for Class-2 saturates at $Th \neq 0$ because of p probability; the tagged node does not compete if the FSO channel is available. The decreasing throughput occurs for higher values of ω_1. Class-2 traffic transition points in throughput occur at region $\omega_1 \in [0.6, 1]$ with decreasing throughput $Th = 0.25$. This is because the RF link access priority increase with decreases in priority of classes.

Fig.4.3 (b) shows Monte Carlo simulation for the same parameters and results shows strong agreement with the analytical model.

In Fig. 4.4, we plot the throughput Th as function of the frame arrival probability ω_1 for different classes traffic with N equal priority users and equal values of buffer size.

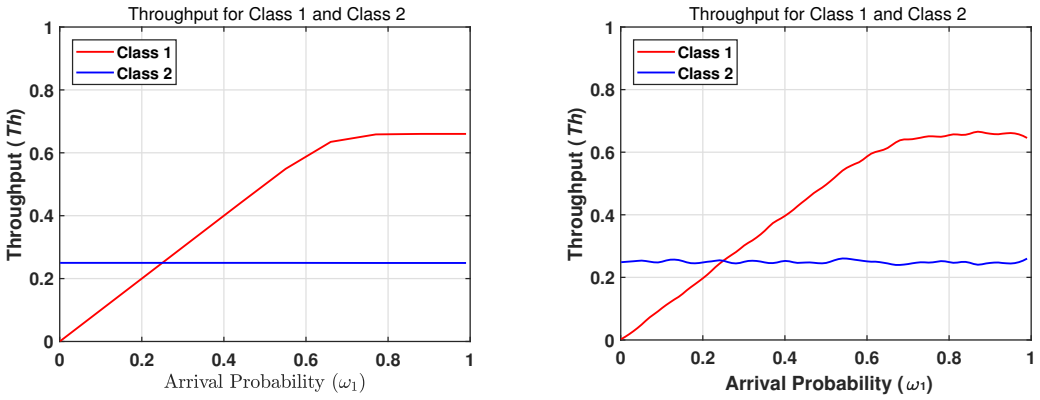

Figure 4.4: Throughput with a = 0.1, b = 0.9, p = 0.5, $\omega_2 = 0.25$, $B_1 = 6$, and $B_2 = 6$ frames. (a) Analytical simulation. (b) Numerical simulation.

We consider $a = 0.1$, $b = 0.9$, the buffer size of each classes traffic is $B = 6$, and p probability value is considered as $p = 0.5$.

It can be seen in Fig.4.4 (a), the throughput graph shows two phases viz linear and saturation. The linear phase occurs at low ω values, while the saturation phase occurs for higher values of ω_1. The transition point occurs when the frame arrival probability $\omega_1 = 0.65$. Class-1 shows the highest throughput because it has the highest priority of accessing the RF link. On the other hand, Class-2 has the lowest priority of accessing the RF link, so it shows the lowest throughput.

For Class-1, the transition from linear to saturation phase occurs when the transmit buffer is not empty. The throughput for Class-1 saturates at $Th = 0.65$ because the RF link is accessed with the probability p and there is no dip in throughput.

The Class-2 starts and remains saturated at $Th = 0.25$ with probability FSO and available RF link. The throughput for Class-2 saturates at $Th \neq 0$ because of p probability; the tagged node does not compete if the FSO channel is available and no dip in throughput because of an equal priority protocol.

4.2.2 Comparison

Comparing the results with the ones obtained in the existing P2MP network, T. Rakia, presents two situations for throughput, when there is no backup RF link and the other situation is using a common backup RF link in [17].

The results show that the saturation phase of the throughput decreases with increasing N. This is due to the increasing competition to access the shared RF link, while the other throughput lines when there is a backup RF link show the improved throughput occur at $Th = 0.8$.

Whereas the results from our P2MP network, Class-1 shows the highest throughput because it has the highest priority of accessing the RF link, the tagged node does not compete if the FSO channel is available. The throughput for Class-1 saturates at a $Th = 0.9$ because the RF link is being accessed with the probability p and there is no dip in throughput. While the Class-2 starts and remains saturated at $Th = 0.5$ with probability FSO and available RF link.

In another P2MP network by N. Lashari. in [44], their results show that Node 1 shows the highest throughput because it has the highest priority of accessing the RF link. Their improved throughput occur at $Th = 0.8$, while node 4 has the lowest priority, so it shows the lowest throughput. There is a dipping phase occur between the lines, this drop is because of non-equal priority protocol.

Our P2MP network results show better results for the same framing rate, the throughput for Class-1 saturates at $Th = 0.9$ and there is no dip in throughput because of an equal priority protocol.

Another P2MP network that uses different rates for transmitting the data frame over the FSO and RF links and p-persistent strategy is presented in [45]. In this P2MP network, using a non-equal priority protocol and p-persistent strategy to improve the performance metrics with equal frame transmission rates of FSO and RF link, the results show that the throughput is entirely linear for all frame arrival probabilities of the highest priority Node 1. A sudden drops in throughput after the linear phase occur for Nodes 2, 3 and 4; the transition occurs when the transmit buffer is not empty and arriving frames can not leave the buffer because access to the RF link is restricted.

In contrast, using the same frame transmission rates of FSO and RF link with an equal priority protocol and choosing class-1 with probability p as a high-priority traffic and class-2 with probability $p-1$ as a low-priority traffic, the results of existing

network show considerable improvements comparing with mentioned networks.

In this section we evaluated that under foggy weather conditions and no rain the transition point in throughput occurs at lower values of ω_1 for a high values of p probability. The throughput for Class-1 traffic is the highest with the high values of p probability and the highest priority of accessing the RF link with an equal priority protocol. It can be seen that using a p probability with an equal priority protocol had improved the throughput.

4.3 Average Buffer Size Q_a Results and Discussion

In this section, we present selected numerical examples to illustrate our analysis introduced in Chapter 3. The results of this existing P2MP network are also compared with an efficient P2MP networks presented in [17], [44] and [45].

4.3.1 Simulation Results

In Fig. 4.5, we plot the average buffer size Q_a as function of the frame arrival probability ω_1 for two classes traffic with N equal priority users. The results obtained with existing P2MP network are compared with some of the results from previous mentioned networks at the end of this section.

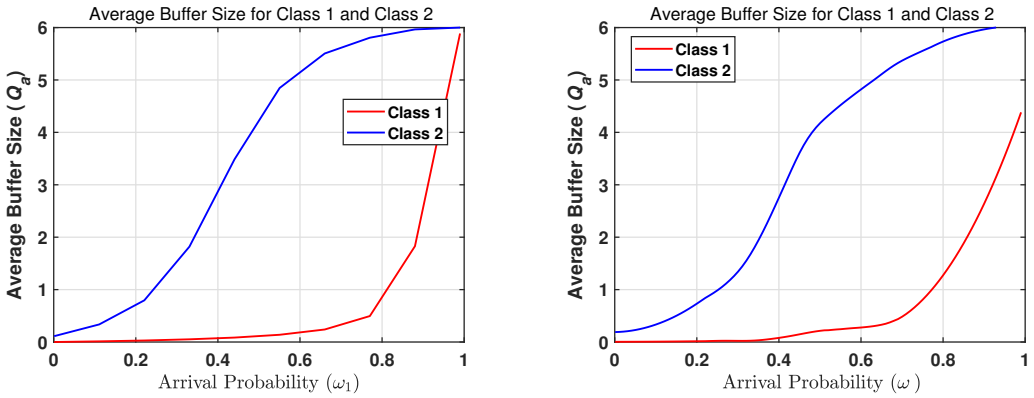

Figure 4.5: Average Buffer Size with a = 0.1, b = 0.9, p = 1, $\omega_2 = 0.5$, $B_1 = 6$, and $B_2 = 6$ frames. (a) Analytical simulation. (b) Numerical simulation.

We consider $a = 0.1$, $b = 0.9$, the buffer size of each classes traffic is $B = 6$, and the p probability value is considered as $p = 1$.

It can be seen in Fig. 4.5 (a), the Q_a graph for Class-1 traffic, the buffer starts filling at high frame arrival probabilities $\omega_1 = 0.8$ when there is a backup RF link with N equal priority users. This is because the central node uses the backup RF link. The average buffer size Q_a increases with smaller values of $\omega_1 = 0.2$ as the priority increase. The average buffer size Q_a saturates at the maximum buffer size B as expected.

The second case is for Class-2 traffic when there is no backup RF link, because of having the lowest priority to access RF link. In this situation, the buffer starts filling at low frame arrival probabilities. This is because the FSO link is in bad quality due to the foggy weather. The average buffer size Q_a saturates at the maximum buffer size B as expected.

Fig. 4.5 (b) shows Monte Carlo simulation for the same parameters and results shows strong agreement with the analytical model.

In Fig. 4.6, we plot the average buffer size Q_a as function of the frame arrival probability ω_1 for two classes traffic with N equal priority users.

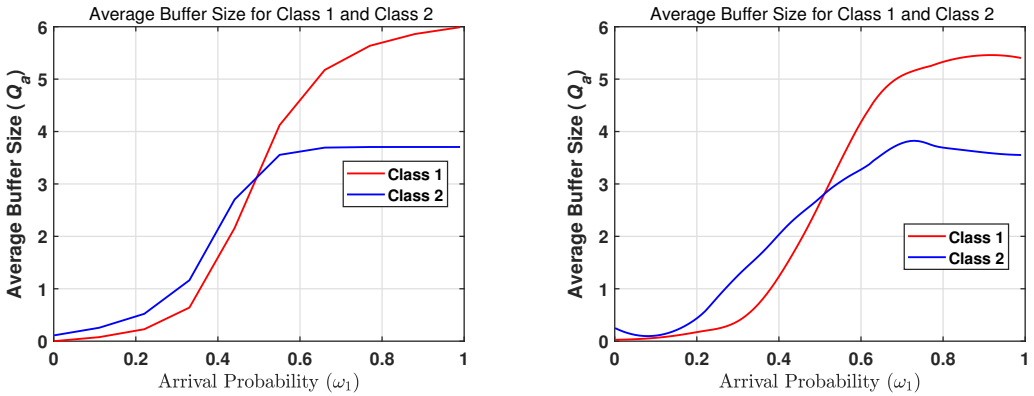

Figure 4.6: Average Buffer Size with a = 0.1, b = 0.9, p = 0.5, $\omega_2 = 0.5$, $B_1 = 6$, and $B_2 = 6$ frames. (a) Analytical simulation. (b) Numerical simulation.

We consider $a = 0.1$, $b = 0.9$, the buffer size of each classes traffic is $B = 6$, and the p probability value is considered as $p = 0.5$.

It can be seen in Fig. 4.6 (a) the Q_a graph for Class-1 traffic, the buffer starts filling at low frame arrival probabilities $\omega_1 = 0.3$. This is because Class-1 has the highest priority to access the RF link.

The special case for Class-2 traffic will have the least average buffer size $Q_a = 3.5$, because of having the lowest priority to access RF link. The buffer starts filling at

low frame arrival probabilities $\omega_1 = 0.3$. The average buffer size Q_a saturates at the maximum buffer size B as expected.

Fig. 4.6 (b) shows Monte Carlo simulation for the same parameters. The strong similarities between the analytical and numerical results prove our analytical model to be accurate.

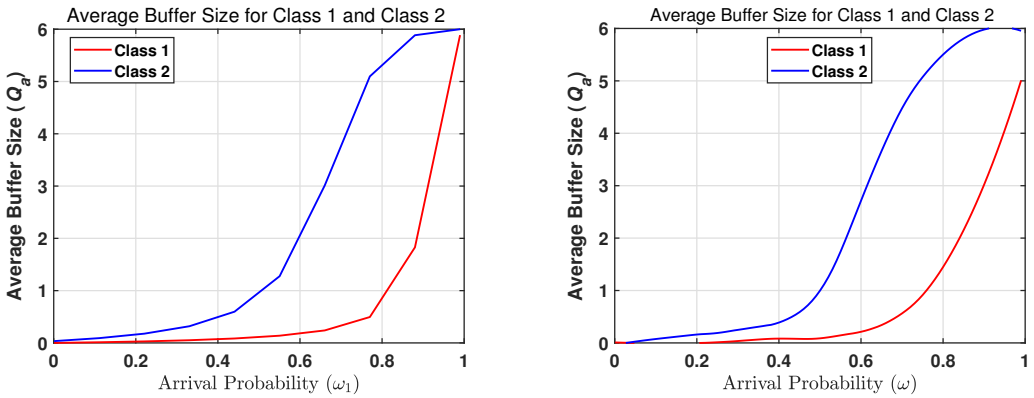

Figure 4.7: Average Buffer Size with a = 0.1, b = 0.9, p = 1, $\omega_2 = 0.25$, $B_1 = 6$, and $B_2 = 6$ frames. (a) Analytical simulation. (b) Numerical simulation.

In Fig. 4.7, we plot the average buffer size Q_a as function of the frame arrival probability ω_1 for two classes traffic with N equal priority users.

We consider $a = 0.1$, $b = 0.9$, the buffer size of each classes traffic is $B = 6$, and the p probability value is considered as $p = 1$.

It can be seen in Fig. 4.7 (a), the Q_a graph for Class-1 traffic, the buffer starts filling at high frame arrival probabilities $\omega_1 = 0.75$ when there is a backup RF link with N equal priority users. This is because the central node uses the backup RF link. The average buffer size Q_a increases with smaller values of $\omega_1 = 0.2$ as the priority increase. The average buffer size Q_a saturates at the maximum buffer size B as expected.

The second case is for Class-2 traffic when there is no backup RF link, because of having the lowest priority to access RF link. In this situation, the buffer starts filling at low frame arrival probability. This is because the FSO link is in bad quality due to the foggy weather. The average buffer size Q_a saturates at the maximum buffer size B as expected.

Fig. 4.7 (b) shows Monte Carlo simulation for the same parameters and results shows strong agreement with the analytical model.

In Fig. 4.8, we plot the average buffer size Q_a as function of the frame arrival probability ω_1 for two classes traffic with N equal priority users.

We consider $a = 0.1$, $b = 0.9$, the buffer size of each classes traffic is $B = 6$, and the p probability value is considered as $p = 0.5$.

It can be seen in Fig. 4.8 (a) the Q_a graph for Class-1 traffic, the buffer starts filling at low frame arrival probabilities $\omega_1 = 0.4$. This is because Class-1 has the highest priority to access the RF link.

The special case for Class-2 traffic will have the least average buffer size $Q_a = 0.5$, because of having the lowest priority to access RF link. The buffer starts filling at low frame arrival probabilities $\omega_1 = 0.2$. The average buffer size Q_a saturates at the maximum buffer size B as expected.

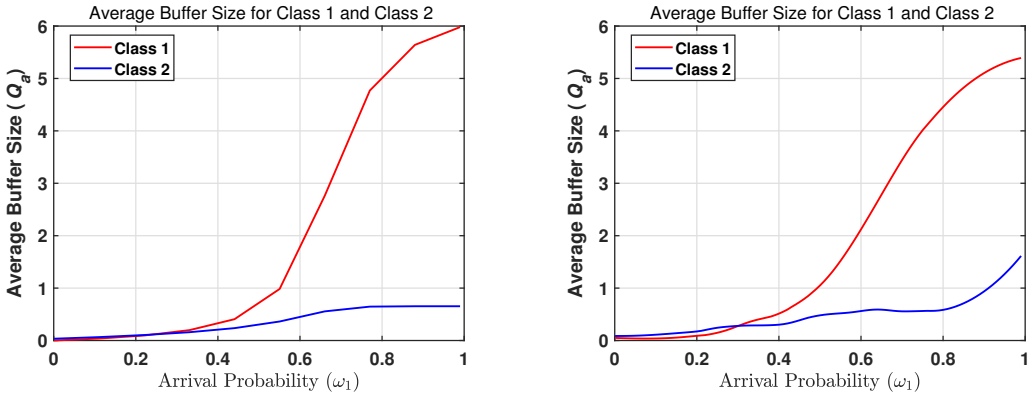

Figure 4.8: Average Buffer Size with a = 0.1, b = 0.9, p = 0.5, $\omega_2 = 0.25$, $B_1 = 6$, and $B_2 = 6$ frames. (a) Analytical simulation. (b) Numerical simulation.

Fig. 4.8 (b) shows Monte Carlo simulation for the same parameters. The strong similarities between the analytical and numeric results prove our analytical model to be accurate.

4.3.2 Comparison

Comparing the results with the ones obtained in the existing P2MP network, T. Rakia, shows two situations, when there is no backup RF link and the other is when there is backup RF link and only one remote node [17]. In first case the buffer starts filling at low symbol arrival probabilities $\omega_1 = 0.1$ because the FSO link is in bad

quality, while the second case shows improved result, the buffer starts filling at high symbol arrival probabilities $\omega_1 = 0.6$.

Whereas the results from our P2MP network, Class-1 shows the best improved result, the buffer starts filling at high symbol arrival probabilities $\omega_1 = 0.8$ and the average buffer size Q_a increases with smaller values of $\omega_1 = 0.2$ as the priority increase. The second case for Class-2 traffic shows better result comparing with mentioned network, the buffer starts filling at low frame arrival probabilities because of having the lowest priority to access RF link $\omega_1 = 0.2$. The average buffer size Q_a saturates at the maximum buffer size $B = 6$ for both cases as expected, the results of existing network show great improvements comparing with mentioned networks.

In another P2MP network by N. Lashari. in [44], their results show that the buffer is transmitting the packet immediately after receiving them, so its buffer size does not increase for the highest priority Node 1, while Node 4 has the lowest priority of using the RF link, so the buffer size increases.

Our P2MP network results show better results for the same framing rate, the average buffer size Q_a increases with smaller values of $\omega_1 = 0.2$ as the priority increase for class-1 traffic and the lowest priority class-2 traffic starts filling at $\omega_1 = 0.2$. The average buffer size Q_a saturates at the maximum buffer size $B = 6$ for both cases as expected.

Another P2MP network that uses different rates and p-persistent strategy shows that the buffer starts filling at high values of $\omega_1 = 0.8$, because Node 1 has the highest priority to access the RF link, while buffer starts filling at low values $\omega_1 = 0.1$ of the lowest priority [45]. On the other hand, using the same frame transmission rates of FSO and RF link with an equal priority protocol, the results of existing network show great improvements comparing with mentioned networks.

In this section we evaluated that under foggy weather conditions and no rain, the transmit buffer with an equal priority users starts filling at lower values of ω_1 for higher values of p probability.

4.4 Average Buffer Queuing Delay T_q Results and Discussion

In this section, we present selected numerical examples to illustrate our analysis introduced in Chapter 3. The results of this existing P2MP network are also compared with an efficient P2MP networks presented in [17], [44] and [45].

4.4.1 Simulation Results

We plot the average queuing delay T_q as function of the frame arrival probability ω_1 for different classes traffic with N equal priority users. The average queuing delay starts at low values then starts increasing after a certain frame arrival probability value ω_1. The delay increases with increasing traffic ω_1 and a high values of p probability.

In Fig. 4.9, We consider $a = 0.1$, $b = 0.9$, the buffer size of each classes traffic is $B = 6$, and the p probability value is considered as $p = 1$.

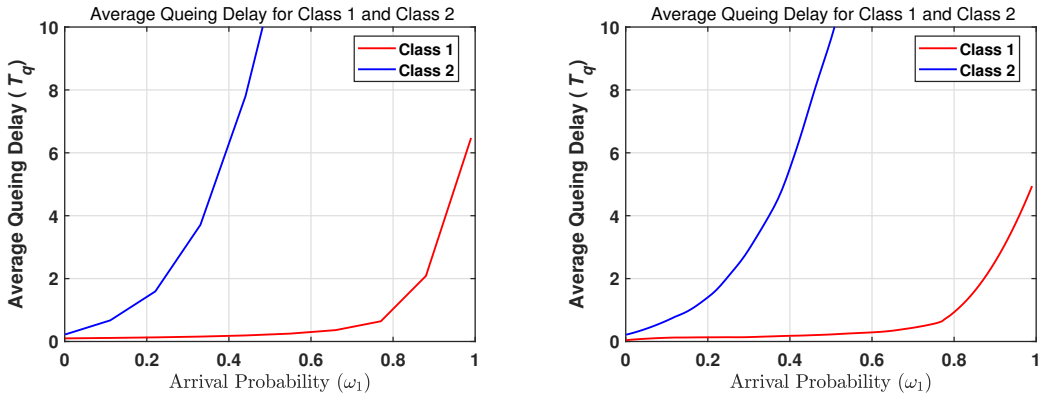

(a) (b)

Figure 4.9: Average queuing delay with a = 0.1, b = 0.9, p = 1, $\omega_2 = 0.5$, $B_1 = 6$, and $B_2 = 6$ frames. (a) Analytical simulation. (b) Numerical simulation.

The best performance occurs for the case of Class-1 traffic because of having highest priority to access backup RF link. The worst performance occurs for Class-2 traffic because of having the lowest access to RF link.

It can be seen Fig. 4.9 (a), Class-1 the value of Average buffer delay starts increasing at $\omega_1 = 0.8$ and the $Tq \neq 0$; this is because of the p probability, every incoming frame will spend some time in the buffer before being transmitted. Class-2 traffic starts increasing at $\omega_1 = 0.2$ and the $Tq \neq 0$.

Fig. 4.9 (b) shows Monte Carlo simulation for the same parameters. The strong similarities between the analytical and numerical results prove our analytical model to be accurate.

In Fig. 4.10 , We consider $a = 0.1$, $b = 0.9$, the buffer size of each classes traffic is $B = 6$, and the p probability value is considered as $p = 0.5$.

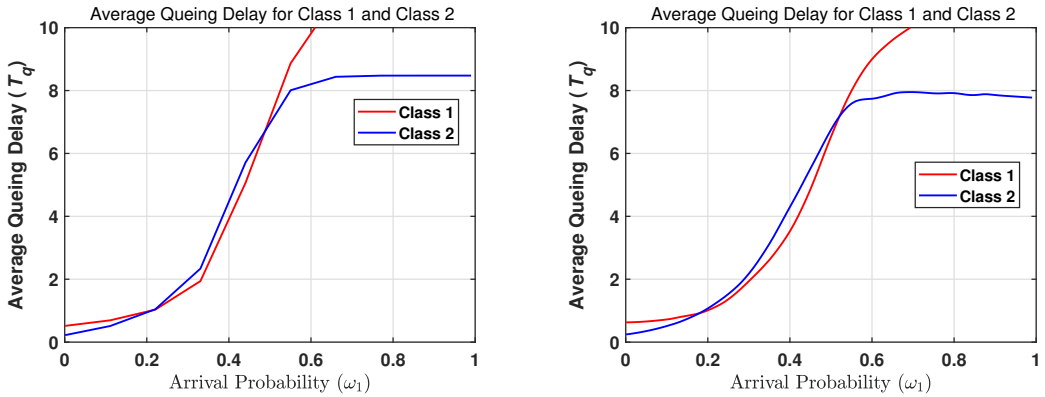

Figure 4.10: Average queuing delay with a = 0.1, b = 0.9, p = 0.5, $\omega_2 = 0.5$, $B_1 = 6$, and $B_2 = 6$ frames. (a) Analytical simulation. (b) Numerical simulation.

The best performance occurs for the case of Class-1 traffic because of having highest priority to access backup RF link. The worst performance occurs for Class-2 traffic because of having the lowest access to RF link.

It can be seen in Fig. 4.10 (a), Class-1 the value of Average buffer delay starts increasing at $\omega_1 = 0.2$ and the $Tq \neq 0$ for all the nodes; this is because of the p probability, every incoming frame will spend some time in the buffer before being transmitted.

Fig. 4.10 (b) shows Monte Carlo simulation for the same parameters. The numerical results strongly coincide with analytical results, proving our analytical model to be accurate.

In Fig. 4.11, We consider $a = 0.1$, $b = 0.9$, the buffer size of each classes traffic is $B = 6$, and the p probability value is considered as $p = 1$.

The best performance occurs for the case of Class-1 traffic because of having highest priority to access backup RF link. The worst performance occurs for Class-2 traffic because of having the lowest access to RF link.

It can be seen Fig. 4.11 (a), Class-1 the value of Average buffer delay starts increasing at $\omega_1 = 0.7$ and the $Tq \neq 0$; this is because of the p probability, every

incoming frame will spend some time in the buffer before being transmitted. Class-2 traffic starts increasing at $\omega_1 = 0.2$ and the $Tq \neq 0$.

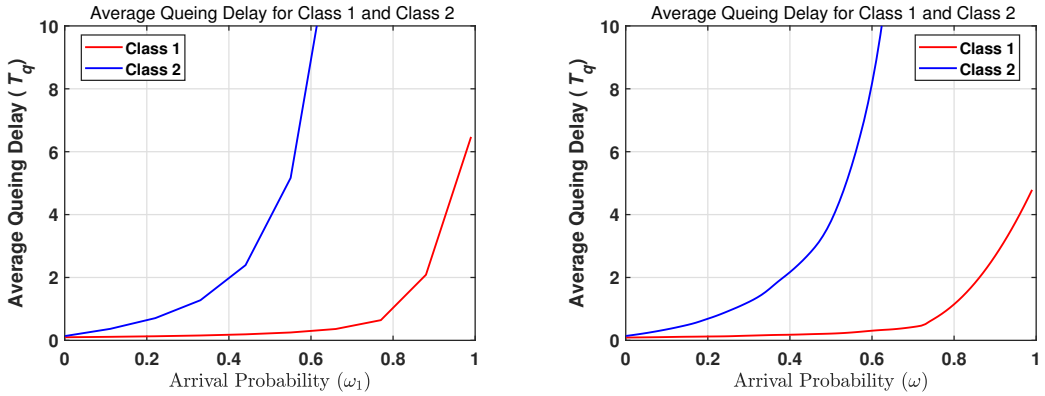

(a) (b)

Figure 4.11: Average queuing delay with a = 0.1, b = 0.9, p = 1, $\omega_2 = 0.25$, $B_1 = 6$, and $B_2 = 6$ frames. (a) Analytical simulation. (b) Numerical simulation.

Fig. 4.11 (b) shows Monte Carlo simulation for the same parameters. The strong similarities between the analytical and numeric results prove our analytical model to be accurate.

In Fig. 4.12 , We consider $a = 0.1$, $b = 0.9$, the buffer size of each classes traffic is $B = 6$, and the p probability value is considered as $p = 0.5$.

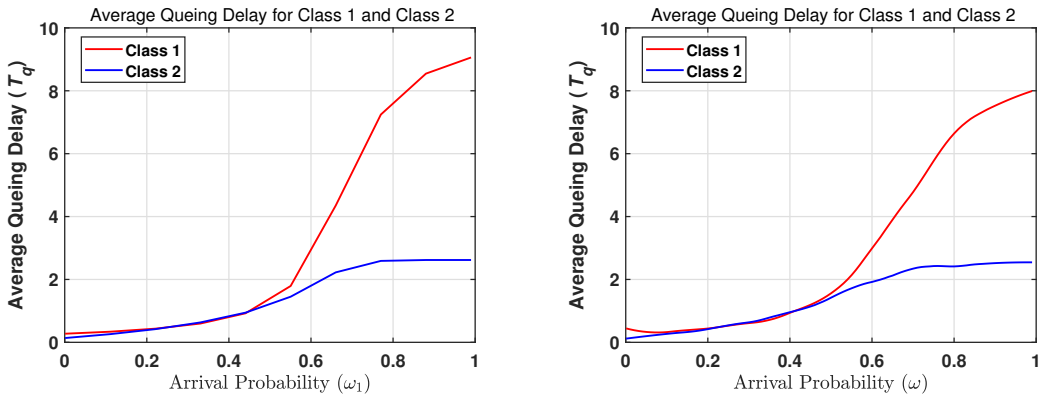

(a) (b)

Figure 4.12: Average queuing delay with a = 0.1, b = 0.9, p = 0.5, $\omega_2 = 0.25$, $B_1 = 6$, and $B_2 = 6$ frames. (a) Analytical simulation. (b) Numerical simulation.

The best performance occurs for the case of Class-1 traffic because of having

highest priority to access backup RF link. The worst performance occurs for Class-2 traffic because of having the lowest access to RF link.

It can be seen in Fig. 4.10 (a), Class-1 the value of Average buffer delay starts increasing at $\omega_1 = 0.3$ and the $Tq \neq 0$ for all the nodes; this is because of the p probability, every incoming frame will spend some time in the buffer before being transmitted.

Fig. 4.12 (b) shows Monte Carlo simulation for the same parameters. The numerical results strongly coincide with analytical results, proving our analytical model to be accurate.

4.4.2 Comparison

The results obtained from the existing network are compared with the results from previous work. The average queuing delay T_q by T. Rakia, shows an S-type behavior, it starts at low values then increasing with increasing values of N, then saturates [17]. The best result occurs when there is a single remote node with a backup RF line, while the worst result occurs when using the FSO links only without a backup RF link, so that the symbol will wait until the FSO link becomes available. However, the special case for N = 1 having the least average queuing delay Tq.

On the other hand, In P2MP network by N. Lashari, in [44], the results show the highest priority Node 1 get preference while accessing the RF link but has lowest queuing delay. In contrast, The behavior of average queuing delay shows that, it initially increases as packets arrive at the node and it then saturates the lowest priority Node 4 has the highest queuing delay.

In another P2MP network by Y. A. Ansari, in [45], the results show that the delay increases with increasing number of nodes and traffic ω. However, for equal frame transmission rates of FSO and RF link, the access to the RF link for a node is restricted by a node of lower number, which causes the performance to decrease (high values of Average buffer delay for small of values ω) and the best performance occurs for highest priority Node 1.

Whereas the results from our P2MP network, for different classes traffic with N equal priority users and equal frame transmission rates of FSO and RF link, show that The delay increases with increasing traffic ω_1 and a high values of p probability.The best performance occurs for the case of Class-1 traffic because of having highest priority to access backup RF link at $\omega_1 = 0.8$ and the $Tq \neq 0$, while he worst

performance occurs for Class-2 traffic because of having the lowest access to RF link $\omega_1 = 0.2$ and the $Tq \neq 0$.

In result, our P2MP network show better results compared with the mentioned Networks with the same frame transmission rates of FSO and RF link and existing Parameters, and in many times, they require less computation. However, the existing P2MP network still offer satisfactory results with considerable improvement of the performance metrics.

In this section we evaluated that under foggy weather conditions and no rain the Average buffer queuing delay starts increasing at lower values of ω_1 for high value of p probability, as incoming traffic increases buffer queuing delay also increases for both classes.

4.5 Frame Loss Probability P_L Results and Discussion

In this section, we present selected numerical examples to illustrate our analysis introduced in Chapter 3. The results of this existing P2MP network are also compared with an efficient P2MP networks presented in [17], [44] and [45].

4.5.1 Simulation Results

We plot the frame loss probability P_L as function of the frame arrival probability ω_1 for different classes traffic with N equal priority users.

The frame loss probability goes into two phases viz zero loss and linear. The zero loss phase occurs at low ω_1 values. The linear phase occurs for higher values of ω_1. The transition point occurs when the buffer is full with probability $s_B \gg 0$. This condition is equivalent to the condition $s_0 = 0$, this condition occurs when $\rho = 1$. This occurs when the frame arrival probability $\omega_1 = z_{1,2}$. Therefore, the zero loss phase of the frame loss probability occurs in the region $\omega_1 \in [0, z_{1,2}]$. The linear phase of the frame loss probability occurs in the region $\omega_1 \in [z_{1,2}, 1]$.

In Fig. 4.13, We consider $a = 0.1$, $b = 0.9$, the buffer size of each classes traffic is $B = 6$, and the p probability value is considered as $p = 1$.

It can be seen in Fig. 4.13 (a), that Class-1 shows zero loss from $\omega_1 = 0$ until $\omega_1 = 0.9$. This is because Class-1 has the highest priority to access the RF link and to transmit the frame. The linear phase of the frame loss probability occurs when the

buffer starts filling up at $\omega_1 = 0.9$ until $\omega_1 = 1$ with $P_L = 0.1$. The worst performance occurs for Class-2 traffic because of having the lowest access to RF link, It goes from zero to linear phase at $\omega_1 = 0.3$ and starts filing up at $\omega_1 = 0.3$ with at most $P_L = 1$.

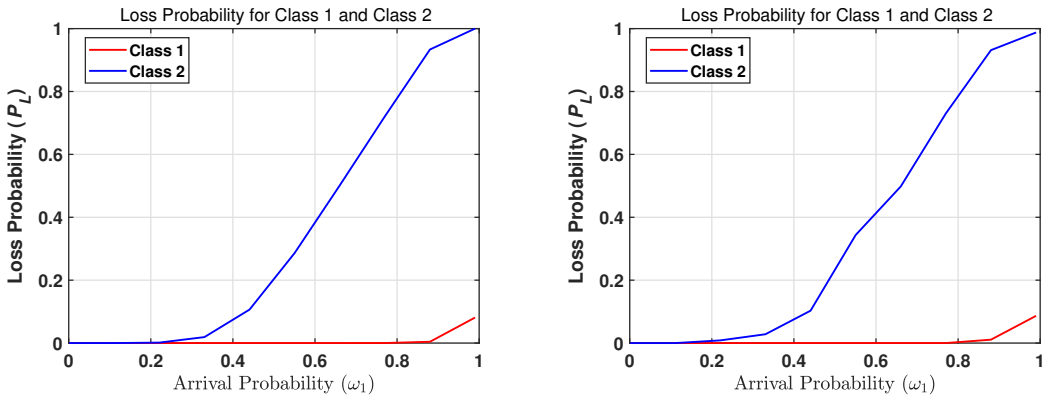

Figure 4.13: Frame Loss Probability with a = 0.1, b = 0.9, p = 1, $\omega_2 = 0.5$, $B_1 = 6$, and $B_2 = 6$ frames. (a) Analytical simulation. (b) Numerical simulation.

Fig. 4.13 (b) shows Monte Carlo simulation for the same parameters. The strong similarities between the analytical and numerical results prove our model to be accurate.

In Fig. 4.14, We consider $a = 0.1$, $b = 0.9$, the buffer size of each classes traffic is $B = 6$, and the p probability value is considered as $p = 0.5$.

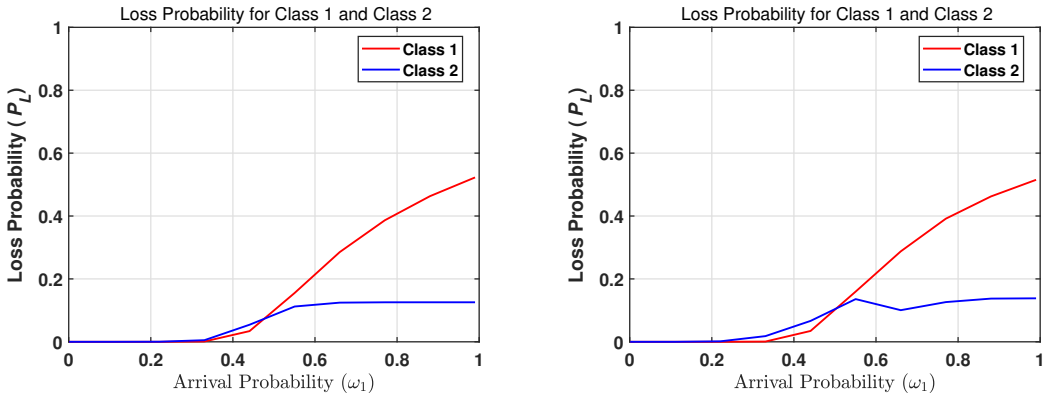

Figure 4.14: Frame Loss Probability with a = 0.1, b = 0.9, p = 0.5, $\omega_2 = 0.5$, $B_1 = 6$, and $B_2 = 6$ frames. (a) Analytical simulation. (b) Numerical simulation.

It can be seen in Fig. 4.14 (a), Class-1 shows zero loss from $\omega_1 = 0$ until $\omega_1 = 0.4$. This is because Class-1 has the highest priority to access the RF link and to transmit the frame. The linear phase of the frame loss probability occurs when the buffer starts filling up at $\omega_1 = 0.4$ until $\omega_1 = 1$ with $P_L = 0.5$.

The worst performance occurs for Class-2 traffic because of having the lowest access to RF link, It goes from zero to linear phase at $\omega_1 = 0.4$ and starts filing up at $\omega_1 = 0.4$ with at most $P_L = 0.1$.

Fig. 4.14 (b) shows Monte Carlo simulation for the same parameters. The strong similarities between the analytical and numerical results prove our model to be accurate.

In Fig. 4.15, We consider $a = 0.1$, $b = 0.9$, the buffer size of each classes traffic is $B = 6$, and the p probability value is considered as $p = 1$.

It can be seen in Fig. 4.15 (a), that Class-1 shows zero loss from $\omega_1 = 0$ until $\omega_1 = 0.9$. This is because Class-1 has the highest priority to access the RF link and to transmit the frame. The linear phase of the frame loss probability occurs when the buffer starts filling up at $\omega_1 = 0.9$ until $\omega_1 = 1$ with $P_L = 0.1$.

The worst performance occurs for Class-2 traffic because of having the lowest access to RF link, It goes from zero to linear phase at $\omega_1 = 0.3$ and starts filing up at $\omega_1 = 0.3$ with at most $P_L = 1$.

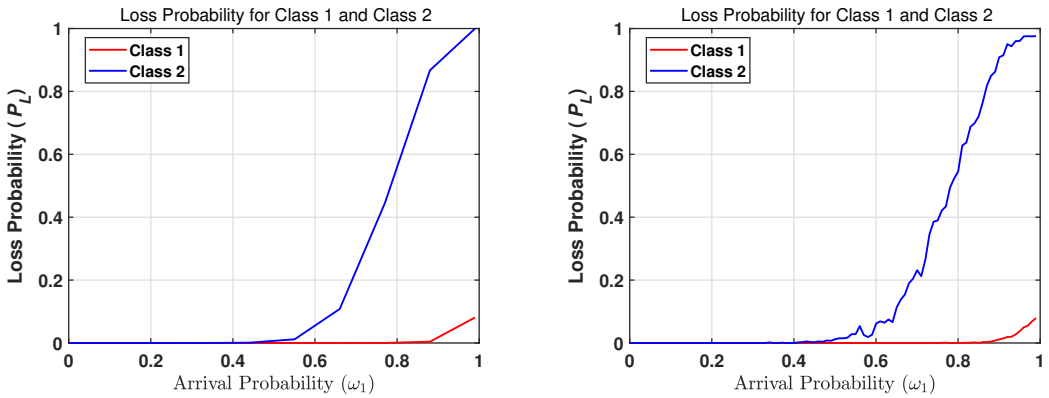

Figure 4.15: Frame Loss Probability with a = 0.1, b = 0.9, p = 1, $\omega_2 = 0.25$, $B_1 = 6$, and $B_2 = 6$ frames. (a) Analytical simulation. (b) Numerical simulation.

Fig. 4.15 (b) shows Monte Carlo simulation for the same parameters. The strong similarities between the analytical and numerical results prove our model to be accurate.

In Fig. 4.16, We consider $a = 0.1$, $b = 0.9$, the buffer size of each classes traffic is $B = 6$, and the p probability value is considered as $p = 0.5$.

It can be seen in Fig. 4.16 (a), Class-1 shows zero loss from $\omega_1 = 0$ until $\omega_1 = 0.4$. This is because Class-1 has the highest priority to access the RF link and to transmit the frame. The linear phase of the frame loss probability occurs when the buffer starts filling up at $\omega_1 = 0.4$ until $\omega_1 = 1$ with $P_L = 0.5$.

The worst performance occurs for Class-2 traffic because of having the lowest access to RF link, It goes from zero to linear phase at $\omega_1 = 0.4$ and starts filing up at $\omega_1 = 0.4$ with at most $P_L = 0.1$.

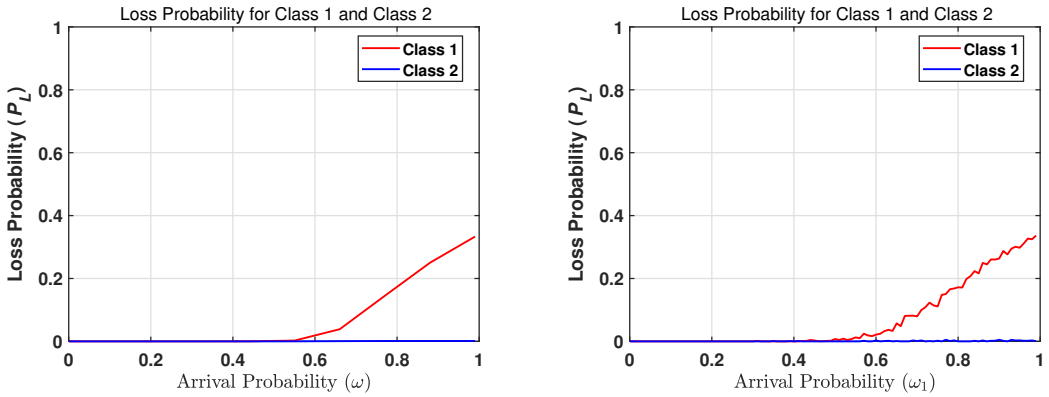

Figure 4.16: Frame Loss Probability with a = 0.1, b = 0.9, p = 0.5, $\omega_2 = 0.25$, $B_1 = 6$, and $B_2 = 6$ frames. (a) Analytical simulation. (b) Numerical simulation.

Fig. 4.16 (b) shows Monte Carlo simulation for the same parameters. The strong similarities between the analytical and numerical results prove our model to be accurate.

4.5.2 Comparison

Comparing the results with the ones obtained in mentioned network presented in [17], The frame loss probability P_L by T. Rakia, shows the graph goes into two phases viz zero loss and linear. The zero loss phase occurs at low ω values, the linear phase occurs for higher values of $\omega = 0.8$ with $P_L = 0.2, 0.7 and 0.8$, while the transition point occurs when the buffer is full.

On the other hand, In P2MP network by N. Lashari, in [44], the results show two phases viz zero loss and linear. The highest priority Node 1 in the graph has low

packet loss probability $\omega = 0.8$ with $P_L = 0.2$, while Node 4 has the highest packet loss $\omega = 0.2$ with $P_L = 1$, this is because it has the least probability of accessing the RF link.

In another P2MP network by Y. A. Ansari, in [45], the results show two phases viz zero loss and linear. The highest priority Node 1 in the graph has zero loss $P_L = 0$, while Node 4 has the highest packet loss $\omega = 0.25$ with $P_L = 1$, this is because it has the least probability of accessing the RF link.

Another results when using the persistent probability show the highest priority Node 1 in the graph has low packet loss probability $\omega = 0.5$ with $P_L = 0.5$ and $\omega = 0.25$ with $P_L = 0.7$, while Node 4 has the highest packet loss $\omega = 0.2$ with $P_L = 0.9$ and $\omega = 0.1$ with $P_L = 0.9$, this is because it has the least probability of accessing the RF link.

Whereas the results from our P2MP network, for different classes traffic with N equal priority users and equal frame transmission rates of FSO and RF link, show that the frame loss probability P_L goes into two phases viz zero loss and linear. The highest priority class-1 in the graph has low frame loss probability $\omega = 0.9$ with $P_L = 0.1$ and $\omega = 0.4$ with $P_L = 0.55$.

Class-2 has the highest frame loss $\omega = 0.3$ with $P_L = 1$ and $\omega = 0.6$ with $P_L = 1$, this is because it has the least probability of accessing the RF link. However, the results obtained from the existing network show great improvements comparing with mentioned networks.

In this section we evaluated that under foggy weather conditions and no rain the transition point in loss probability occurs at lower values of ω_1 for high values of p probability. As incoming traffic increases loss probability also increases for both classes.

4.6 Efficiency φ Results and Discussion

In this section, we present selected numerical examples to illustrate our analysis introduced in Chapter 3. The results of this existing P2MP network are also compared with an efficient P2MP networks presented in [17], [44] and [45].

4.6.1 Simulation Results

We plot the efficiency φ as function of the frame arrival probability ω_1 for different classes traffic with N equal priority users. The efficiency φ goes into two phases viz unity efficiency and decreasing efficiency. The unity efficiency phase occurs at low ω_1 values. The decreasing efficiency occurs for higher values of ω_1. The transition point occurs when the buffer is not empty.

In Fig. 4.17, We consider $a = 0.1$, $b = 0.9$, the buffer size of each classes traffic is $B = 6$, and p probability value is considered as $p = 1$.

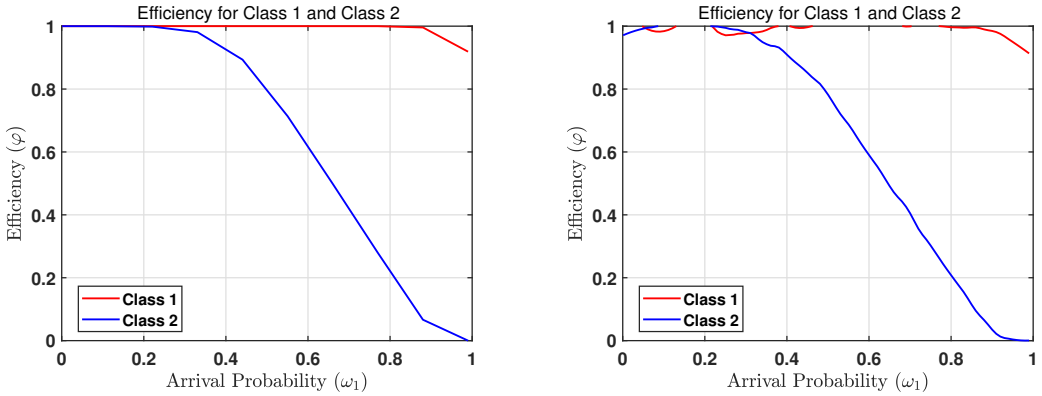

Figure 4.17: Efficiency with a = 0.1, b = 0.9, p = 1, $\omega_2 = 0.5$, $B_1 = 6$, and $B_2 = 6$ frames. (a) Analytical simulation. (b) Numerical simulation.

It can be seen in Fig. 4.17 (a), that Class-1 shows the unity efficiency phase occurs in the region $\omega_1 \in [0, 0.9]$. This is because Class-1 has the highest priority to access the RF link and to transmit the frame. Class-1 traffic transition points in efficiency occur at region $\omega_1 \in [0.9, 1]$ with decreasing efficiency $\varphi = 0.9$. This is because the RF link access priority decreases with increase in priority of classes.

Class-2 shows the unity efficiency phase occurs in the region $\omega_1 \in [0, 0.35]$, this because of having the lowest access to RF link. Class-2 traffic transition points in

efficiency occur at region $\omega_1 \in [0.35, 1]$.

Fig. 4.17 (b) shows Monte Carlo simulation for the same parameters and results show strong agreement with the analytical model.

In Fig. 4.18, We consider $a = 0.1$, $b = 0.9$, the buffer size of each classes traffic is $B = 6$, and p probability value is considered as $p = 0.5$.

It can be seen in Fig. 4.18(a),that Class-1 shows the unity efficiency phase occurs in the region $\omega_1 \in [0, 0.4]$, this occurs when the frame arrival probability $\omega_1 = z_{1,2}$. This is because Class-1 has the highest priority to access the RF link and to transmit the frame. Class-1 traffic transition points in efficiency occur at region $\omega_1 \in [0.4, 1]$ with decreasing efficiency $\varphi = 0.5$. This is because the RF link access priority decreases with increase in priority of classes.

Class-2 shows the unity efficiency phase occurs in the region $\omega_1 \in [0, 0.35]$, this because of having the lowest access to RF link. Class-2 traffic transition points in efficiency occur at region $\omega_1 \in [0.35, 1]$ with decreasing efficiency $\varphi = 0.9$.

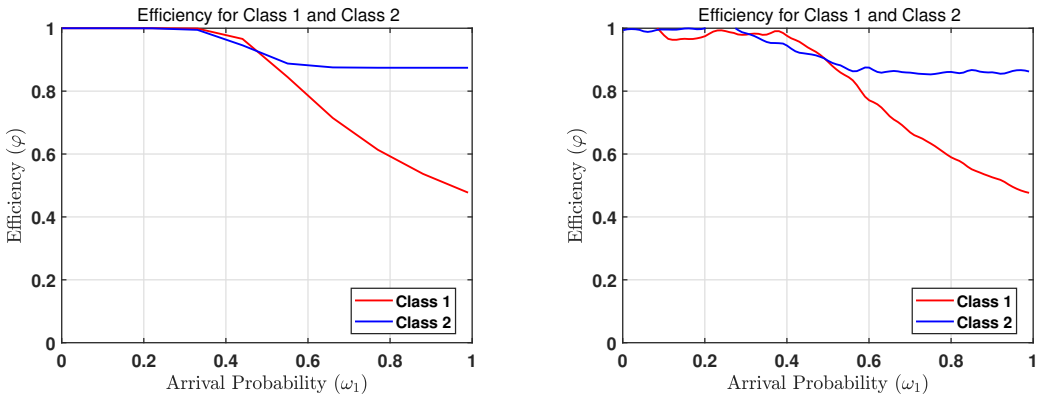

Figure 4.18: Efficiency with a = 0.1, b = 0.9, p = 0.5, $\omega_2 = 0.5$, $B_1 = 6$, and $B_2 = 6$ frames. (a) Analytical simulation. (b) Numerical simulation.

Fig. 4.18 (b) shows Monte Carlo simulation for the same parameters and results show strong agreement with the analytical model.

In Fig. 4.19, We consider $a = 0.1$, $b = 0.9$, the buffer size of each classes traffic is $B = 6$, and p probability value is considered as $p = 1$.

It can be seen in Fig. 4.19 (a), that Class-1 shows the unity efficiency phase occurs in the region $\omega_1 \in [0, 0.9]$. This is because Class-1 has the highest priority to access the RF link and to transmit the frame. Class-1 traffic transition points in efficiency

occur at region $\omega_1 \in [0.9, 1]$ with decreasing efficiency $\varphi = 0.9$. This is because the RF link access priority decreases with increase in priority of classes.

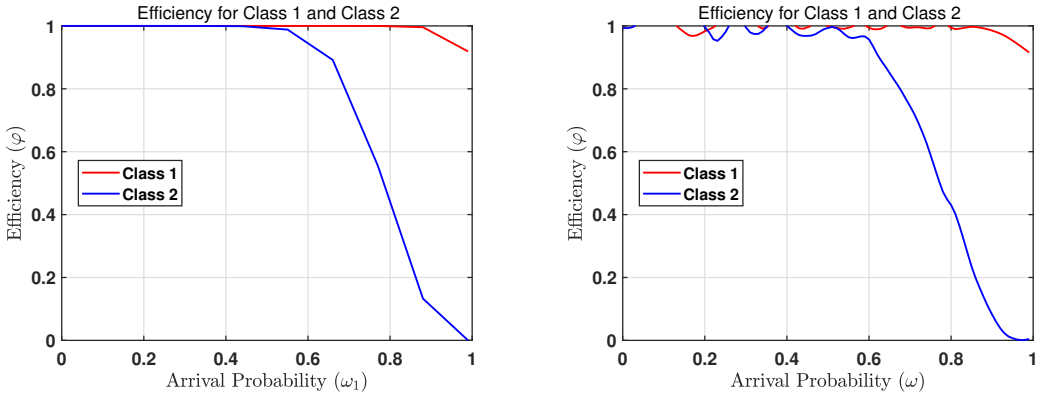

Figure 4.19: Efficiency with a = 0.1, b = 0.9, p = 1, $\omega_2 = 0.25$, $B_1 = 6$, and $B_2 = 6$ frames. (a) Analytical simulation. (b) Numerical simulation.

Class-2 shows the unity efficiency phase occurs in the region $\omega_1 \in [0, 0.5]$, this because of having the lowest access to RF link. Class-2 traffic transition points in efficiency occur at region $\omega_1 \in [0.5, 1]$.

Fig. 4.19 (b) shows Monte Carlo simulation for the same parameters and results show strong agreement with the analytical model.

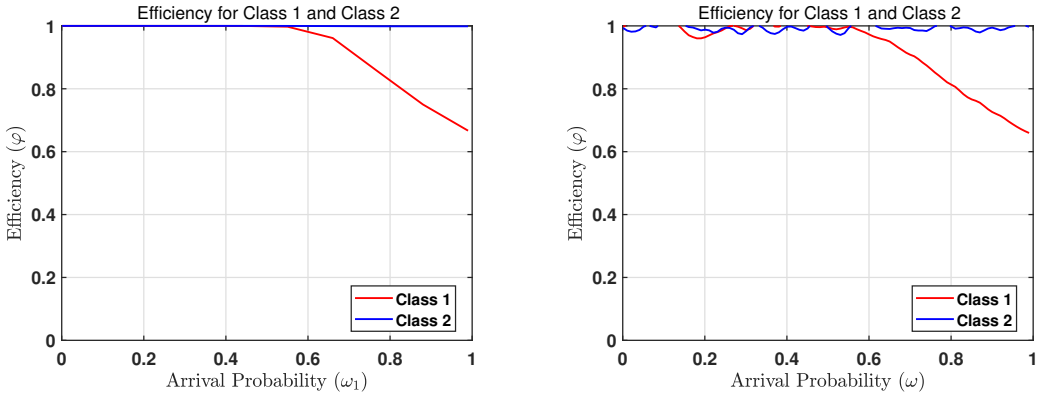

Figure 4.20: Efficiency with a = 0.1, b = 0.9, p = 0.5, $\omega_2 = 0.25$, $B_1 = 6$, and $B_2 = 6$ frames. (a) Analytical simulation. (b) Numerical simulation.

In Fig. 4.20, We consider $a = 0.1$, $b = 0.9$, the buffer size of each classes traffic is

$B = 6$, and p probability value is considered as $p = 0.5$.

It can be seen in Fig. 4.20(a),that Class-1 shows the unity efficiency phase occurs in the region $\omega_1 \in [0, 0.55]$, this occurs when the frame arrival probability $\omega_1 = z_{1,2}$. This is because Class-1 has the highest priority to access the RF link and to transmit the frame. Class-1 traffic transition points in efficiency occur at region $\omega_1 \in [0.55, 1]$ with decreasing efficiency $\varphi = 0.65$. This is because the RF link access priority decreases with increase in priority of classes. The efficiency for class-2 is always unity.

Fig. 4.18 (b) shows Monte Carlo simulation for the same parameters and results show strong agreement with the analytical model.

4.6.2 Comparison

Comparing the results with the ones obtained in mentioned network presented in [17], the efficiency φ by T. Rakia, shows The graph goes into two phases viz unity efficiency occurs at low ω values, and decreasing efficiency occurs for higher values of ω. Further, the efficiency decreases as N increases, due to the increasing competition to access the shared RF link and its clearly that using a common backup RF link had improved the efficiency.

On the other hand, In P2MP network by N. Lashari, in [44], the results show the efficiency φ goes into two phases viz unity efficiency occurs at low ω values, and decreasing efficiency occurs for higher values of ω. Node 1 has the highest priority of accessing the RF link, shows the highest efficiency, because the packets are continuously transmitting. However for the node 4 in the graph has the unity efficiency, but as the packet arrival rate increases, its efficiency goes down due to its low probability of accessing the RF link.

In another P2MP network by Y. A. Ansari, in [45], the results show the efficiency φ goes into two phases viz unity efficiency occurs at low ω values, and decreasing efficiency occurs for higher values of ω. Node 1 shows the highest efficiency because it has the highest priority, The access to the RF link for a node is restricted by a node of lower number.

Another results when using the persistent probability show the highest priority Node 1 goes from unity to decreasing efficiency, which transmits frame with probability p, increasing the chances for a frame being transmitted to all the nodes.

Whereas the results from our P2MP network, for different classes traffic with N

equal priority users and equal frame transmission rates of FSO and RF link, show that the efficiency φ goes into two phases viz unity efficiency occurs at low ω values, and decreasing efficiency occurs for higher values of ω. Class-1 in the graph shows the unity efficiency phase occurs in the region $\omega_1 \in [0, 0.9]$ with decreasing efficiency $\varphi = 0.9$, this is because the RF link access priority decreases with increase in priority of classes. Other results when using different values of p probability and ω_1 show class-1 traffic transition points in efficiency occur at region $\omega_1 \in [0.4, 1]$ with decreasing efficiency $\varphi = 0.5$. This is because the RF link access priority decreases with increase in priority of classes.

Class-2 shows the unity efficiency phase occurs in the region $\omega_1 \in [0, 0.35]$, this because of having the lowest access to RF link. Class-2 traffic transition points in efficiency occur at region $\omega_1 \in [0.35, 1]$ with decreasing efficiency $\varphi = 0.9$. However, the results obtained from the existing network show great improvements comparing with mentioned networks.

In this section we evaluated that under foggy weather conditions and no rain the transition point in φ occurs at lower values of ω_1 for higher values of p probability. As incoming traffic increases, efficiency decreases subject to availability of transmission links.

4.7 Summary

In this chapter, we proposed and analyzed a P2MP Hybrid FSO/RF network. The central node use a common backup RF link for data transmission to any tagged node in case of the failure of its FSO link. The base station reserves two transmit buffers B_1 and B_2 for class-1 and class-2 traffic, respectively.

We studied the performance of a single tagged node (remote node) instead of studying the general system performance. A discrete-time Markov chain model was developed for the transmit buffers of the link between the central node and the remote node. A different performance metrics are defined such as throughput from central node to the remote node for both classes traffic, the average transmit buffer size, the frame queuing delay in both transmit buffer, the efficiency of the queuing system and the frame loss probability.

Numerical examples proved that the P2MP Hybrid FSO/RF network achieves significant performance improvement. Further, using a p probability with an equal priority protocol had improved the performance of proposed P2MP Hybrid network.

Chapter 5

Conclusion and Contributions

In this chapter, the achieved work is summarized, the dissertation contributions and outlines research directions for future work are high-lighted.

5.1 Thesis Contributions

The main goal of this thesis is to study and analysis P2MP Hybrid FSO/RF network over the P2MP FSO-only network; using an equal priority protocol with p probability to improve the system performance. The contributions of this work can be summarized as follow:

1. An-equal priority protocol of P2MP hybrid FSO/RF network for down link traffic is proposed.
2. A Markov chain model of the proposed network is developed.
3. The proposed protocol is modeled using the Monte Carlo method and Several performance metrics are studied.

5.2 Conclusion

The availability of FSO links is restricted by weather conditions. To improve overall system performance and availability, an RF link is firmed in parallel to the FSO link forming a Hybrid FSO/RF system. Since Hybrid free-space optical (FSO)/radio-frequency (RF) communication is achieve higher reliability along with high data rate communication, and since P2MP Hybrid FSO/RF network performs considerable performance improvement over the P2MP FSO only network.

Considering a multi-user scenario, we proposed and analyzed a P2MP Hybrid FSO/RF Network. In this network, the base station use a common backup RF link for data transmission to any user in case of the failure of its FSO link. Thus, it maintains a reliable communication at a reduced data rate. The base station reserves two transmit buffers B_1 and B_2 for class-1 and class-2 traffic, respectively. We studied the performance of a single tagged node (remote node) instead of studying the general system performance.

A discrete-time Markov chain model was developed for the transmit buffers of the link between the central node and the remote node.

A different performance metrics are defined such as throughput from central node to the remote node for both classes traffic, the average transmit buffer size, the frame queuing delay in both transmit buffer, the efficiency of the queuing system and the frame loss probability.

Using an-equal priority protocol with a common backup RF link, and p probability, our proposed P2MP Hybrid FSO/RF network achieves significant performance improvement.

We focused on analytical performance evaluation of the proposed P2MP hybrid FSO/RF network, which will provide important engineering insights into hybrid FSO/RF systems for real world applications and performance calculations.

5.3 Future Work

We have assigned the priorities for the traffic with an equal rates, the future work would be assign priorities to traffic with non equal rates. Also we have assumed that when the FSO link fails, the central node uses a common backup RF link for data transmission, which uses a priority protocol.Using other protocols such as random delay protocol, round robin protocol and delay aware scheduling will effect the Markov chain modeling and can be considered as the future work.

Bibliography

[1] T. Rakia, *Performance analysis of hybrid optical wireless and radio frequency communication systems*. PhD thesis, University of Victoria, Victoria, BC, 2016.

[2] D. Schulz, V. Jungnickel, C. Alexakis, M. Schlosser, J. Hilt, A. Paraskevopoulos, L. Grobe, P. Farkas, and R. Freund, "Robust optical wireless link for the backhaul and fronthaul of small radio cells," *Journal of Lightwave Technology*, vol. 34, no. 6, pp. 1523–1532, 2016.

[3] K. Balaji and K. Prabu, "Performance evaluation of FSO system using wavelength and time diversity over malaga turbulence channel with pointing errors," *Optics Communications*, vol. 410, pp. 643–651, 2018.

[4] J. Abouei and K. N. Plataniotis, "Multiuser diversity scheduling in free-space optical communications," *Journal of Lightwave Technology*, vol. 30, no. 9, pp. 1351–1358, 2012.

[5] Z. Ghassemlooy, W. Popoola, and S. Rajbhandari, *Optical Wireless Communications: System And Channel Modelling With Matlab®*. CRC press, 2012.

[6] Z. Ghassemlooy, S. Arnon, M. Uysal, Z. Xu, and J. Cheng, "Emerging optical wireless communications-advances and challenges," *IEEE Journal On Selected Areas In Communications*, vol. 33, no. 9, pp. 1738–1749, 2015.

[7] A. S. Hamza, J. S. Deogun, and D. R. Alexander, "Classification framework for free space optical communication links and systems," *IEEE Communications Surveys & Tutorials*, vol. 21, no. 2, pp. 1346–1382, 2018.

[8] M. Z. Chowdhury, M. T. Hossan, A. Islam, and Y. M. Jang, "A comparative survey of optical wireless technologies: Architectures and applications," *IEEE Access*, vol. 6, pp. 9819–9840, 2018.

[9] T. Rakia, H.-C. Yang, M.-S. Alouini, and F. Gebali, "Outage analysis of practical FSO/RF hybrid system with adaptive combining," *IEEE Communications Letters*, vol. 19, no. 8, pp. 1366–1369, 2015.

[10] G. N. Kamga and S. Aissa, "Relay selection based hybrid RF/FSO transmission over double generalized gamma channels under outdated CSI and pointing errors," in *2018 IEEE International Conference on Communications (ICC)*, pp. 1–6, IEEE, 2018.

[11] H. Samimi and M. Uysal, "End-to-end performance of mixed RF/FSO transmission systems," *IEEE/OSA Journal of Optical Communications and Networking*, vol. 5, no. 11, pp. 1139–1144, 2013.

[12] L. Chen, W. Wang, and C. Zhang, "Multiuser diversity over parallel and hybrid FSO/RF links and its performance analysis," *IEEE Photonics Journal*, vol. 8, no. 3, pp. 1–9, 2016.

[13] N. Guo, R. C. Qiu, S. S. Mo, and K. Takahashi, "60-Ghz millimeter-wave radio: Principle, technology, and new results," *EURASIP journal on Wireless Communications and Networking*, vol. 2007, no. 1, pp. 48–48, 2007.

[14] S. K. Shrivastava, S. Sengar, and S. P. Singh, "A new switching scheme for hybrid FSO/RF communication in the presence of strong atmospheric turbulence," *Photonic Network Communications*, pp. 1–10, 2018.

[15] M. Usman, H.-C. Yang, and M.-S. Alouini, "Practical switching-based hybrid FSO/RF transmission and its performance analysis," *IEEE Photonics Journal*, vol. 6, no. 5, pp. 1–13, 2014.

[16] T. Rakia, H.-C. Yang, F. Gebali, and M.-S. Alouini, "Power adaptation based on truncated channel inversion for hybrid FSO/RF transmission with adaptive combining," *IEEE Photonics Journal*, vol. 7, no. 4, pp. 1–12, 2015.

[17] T. Rakia, F. Gebali, H.-C. Yang, and M.-S. Alouini, "Cross layer analysis of P2MP hybrid FSO/RF network," *Journal of Optical Communications and Networking*, vol. 9, no. 3, pp. 234–243, 2017.

[18] T. Rakia, F. Gebali, H.-C. Yang, and M.-S. Alouini, "Throughput analysis of point-to-multi-point hybric FSO/RF network," in *Communications (ICC), 2017 IEEE International Conference on*, pp. 1–6, IEEE, 2017.

[19] M. Z. Chowdhury, M. T. Hossan, M. K. Hasan, and Y. M. Jang, "Integrated RF/optical wireless networks for improving qos in indoor and transportation applications," *Wireless Personal Communications*, vol. 107, no. 3, pp. 1401–1430, 2019.

[20] M. A. Amirabadi and V. T. Vakili, "A novel hybrid FSO/RF communication system with receive diversity," *Optik*, vol. 184, pp. 293–298, 2019.

[21] M. Uysal, C. Capsoni, Z. Ghassemlooy, A. Boucouvalas, and E. Udvary, *Optical Wireless Communications: An Emerging Technology*. Springer, 2016.

[22] M. A. Cox, L. Maqondo, R. Kara, G. Milione, L. Cheng, and A. Forbes, "The resilience of hermite-and laguerre-gaussian modes in turbulence," *Journal of Lightwave Technology*, 2019.

[23] W. Rabinovich, C. Moore, H. Burris, J. Murphy, R. Mahon, M. Ferraro, P. Goetz, L. Thomas, C. Font, and Gilbreath, "Free space optical communications research at the us naval research laboratory," in *Free-Space Laser Communication Technologies XXII*, vol. 7587, p. 758702, International Society for Optics and Photonics, 2010.

[24] F. Gebali, *Analysis of computer networks, second edition*. Springer, 2015.

[25] K. Balamurugan, K. Chitra, and A. Jawahar, "Enhanced hierarchical cluster based routing protocol with optical sphere in FSO MANET," in *Optical and Microwave Technologies*, pp. 1–8, Springer, 2018.

[26] Z. Ghassemlooy, W. Popoola, and S. Rajbhandari, *Optical Wireless Communications: System And Channel Modelling With Matlab®*. CRC press, 2019.

[27] S. Mahajan, D. Prakesh, and H. Singh, "Performance analysis of free space optical system under different weather conditions," in *2019 6th International Conference on Signal Processing and Integrated Networks (SPIN)*, pp. 220–224, IEEE, 2019.

[28] A. A. Farid and S. Hranilovic, "Outage capacity optimization for free-space optical links with pointing errors," *Journal of Lightwave Technology*, vol. 25, no. 7, pp. 1702–1710, 2007.

[29] I. S. Ansari, F. Yilmaz, and M.-S. Alouini, "Performance analysis of free-space optical links over málaga ($\mathcal{M}$) turbulence channels with pointing errors.) turbulence channels with pointing errors," *IEEE Transactions on Wireless Communications*, vol. 15, no. 1, pp. 91–102, 2016.

[30] D. K. Borah and D. G. Voelz, "Pointing error effects on free-space optical communication links in the presence of atmospheric turbulence," *Journal of Lightwave Technology*, vol. 27, no. 18, pp. 3965–3973, 2009.

[31] F. E. Goodwin, "A review of operational laser communication systems," *Proceedings of the IEEE*, vol. 58, no. 10, pp. 1746–1752, 1970.

[32] S. Nath, S. K. Shrivastava, S. Sengar, and S. P. Singh, "Novel architectures for efficient rf usage in hybrid FSO/RF system," in *2018 IEEE International Conference on Advanced Networks and Telecommunications Systems (ANTS)*, pp. 1–6, IEEE, 2018.

[33] L. C. Andrews and R. L. Phillips, *Laser beam propagation through random media*, vol. 152. SPIE press Bellingham, WA, 2005.

[34] I. B. Djordjevic and G. T. Djordjevic, "On the high-speed communication over hybrid free-space optical (FSO)-wireless fading channels," in *2009 IEEE LEOS Annual Meeting Conference Proceedings*, pp. 833–834, IEEE, 2009.

[35] N. D. Chatzidiamantis, G. K. Karagiannidis, E. E. Kriezis, and M. Matthaiou, "Diversity combining in hybrid RF/FSO systems with PSK modulation," in *International Conference on Communications (ICC)*, pp. 1–6, IEEE, 2011.

[36] H. Tapse and D. K. Borah, "Hybrid optical/RF channels: characterization and performance study using low density parity check codes," *IEEE Transactions on Communications*, vol. 57, no. 11, pp. 3288–3297, 2009.

[37] S. Mog and R. S. Kshetrimayum, "Performance analysis of sm-based hybrid mimo FSO/RF system,"

[38] K. O. Odeyemi and P. A. Owolawi, "Relay selection in energy harvesting aided mixed rf/fso system with transmit antenna selection over atmospheric turbulence and pointing error," *Progress In Electromagnetics Research*, vol. 97, pp. 139–150, 2019.

[39] S. Nath, S. Sengar, S. K. Shrivastava, and S. P. Singh, "Impact of atmospheric turbulence, pointing error, and traffic pattern on the performance of cognitive hybrid FSO/RF system," *IEEE Transactions on Cognitive Communications and Networking*, vol. 5, no. 4, pp. 1194–1207, 2019.

[40] J. Shi, L. Lv, Q. Ni, H. Pervaiz, and C. Paoloni, "Modeling and analysis of point-to-multipoint millimeter wave backhaul networks," *IEEE Transactions on Wireless Communications*, vol. 18, no. 1, pp. 268–285, 2019.

[41] P. Wang, N. Xiang, Q. Gao, R. Wang, L. Guo, and Y. Yang, "On the performances of n th best user selection scheme in multiuser diversity free-space optical systems over exponentiated weibull turbulence channels," *IEEE Photonics Journal*, vol. 8, no. 2, pp. 1–15, 2016.

[42] S. Zhalehpour, M. Uysal, O. A. Dobre, and T. Ngatched, "Outage capacity and throughput analysis of multiuser FSO systems," in *14th Canadian Workshop on Information Theory (CWIT)*, pp. 143–146, IEEE, 2015.

[43] W. Du, Z. Ji, and Z. Wang, "Self-adaptive truncated binary exponential back-off scheme for WiMAX P2MP network with heavy traffic," in *2008 11th IEEE Singapore International Conference on Communication Systems*, pp. 1652–1656, IEEE, 2008.

[44] N. Lashari, "Performance analysis of hybrid FSO/RF communication system," Master's thesis, University of Victoria, Victoria, BC, 2017.

[45] Y. A. Ansari, "Performance analysis of P2MP hybrid FSO/RF network," Master's thesis, University of Victoria, Victoria, BC, 2017.

[46] M. Haugh, "Generating random variables and stochastic processes," *Monte Carlo Simulation: IEOR EA703*, 2004.